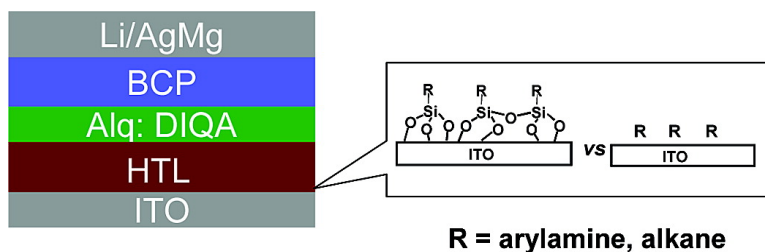Article

Covalently Bound Hole-Injecting Nanostructures. Systematics of Molecular Architecture, Thickness, Saturation, and Electron-Blocking Characteristics on Organic Light-Emitting Diode Luminance, Turn-on Voltage, and Quantum Efficiency

Qinglan Huang, Guennadi A. Evmenenko, Pulak Dutta, Paul Lee, Neal R. Armstrong, and Tobin J. Marks

R = arylamine, alkane

More About This Article

Additional resources and features associated with this article are available within the HTML version:

- Supporting Information
- Links to the 16 articles that cite this article, as of the time of this article download
- Access to high resolution figures
- Links to articles and content related to this article
- Copyright permission to reproduce figures and/or text from this article

View the Full Text HTML

Covalently Bound Hole-Injecting Nanostructures. Systematics of Molecular Architecture, Thickness, Saturation, and Electron-Blocking Characteristics on Organic Light-Emitting Diode Luminance, Turn-on Voltage, and Quantum Efficiency

Qinglan Huang,[†] Guennadi A. Evmenenko,[‡] Pulak Dutta,[‡] Paul Lee,[§]
Neal R. Armstrong,[§] and Tobin J. Marks*,[†]

*Contribution from the Department of Chemistry and the Materials Research Center, and
Department of Physics and Astronomy and the Materials Research Center,
Northwestern University, Evanston, Illinois 60208, and Department of Chemistry and
Optical Science Center, University of Arizona, Tucson, Arizona 85721*

Received February 19, 2005 ; E-mail: t-marks@northwestern.edu

Abstract: Hole transporting materials are widely used in multilayer organic and polymer light-emitting diodes (OLEDs, PLEDs, respectively) and are indispensable if device electroluminescent response and durability are to be truly optimized. This contribution analyzes the relative effects of tin-doped indium oxide (ITO) anode-hole transporting layer (HTL) contact versus the intrinsic HTL materials properties on OLED performance. Two siloxane-based HTL materials, *N,N′*-bis(*p*-trichlorosilylpropyl)-naphthalen-1-yl)-*N,N′*-diphenyl-biphenyl-4,4′-diamine (NPB-Si$_2$) and 4,4′-bis[(*p*-trichlorosilylpropylphenyl)phenylamino]biphenyl (TPD-Si$_2$), are designed and synthesized. They have the same hole transporting triarylamine cores as conventional HTL materials such as 1,4-bis(1-naphthylphenylamino)biphenyl (NPB) and *N,N*-diphenyl-*N,N*-bis(3-methylphenyl)-1,1-biphenyl)-4,4-diamine (TPD), respectively. However, they covalently bind to the ITO anode, forming anode-HTL contacts that are intrinsically different from those of the anode to TPD and NPB. Applied to archetypical tris(8-hydroxyquinolato)aluminum(III) (Alq)-based OLEDs as (1) the sole HTLs or (2) anode-NPB HTL interlayers, NPB-Si$_2$ and TPD-Si$_2$ enhance device electroluminescent response significantly versus comparable devices based on NPB alone. In the first case, OLEDs with 36 000 cd/m^2 luminance, 1.6% forward external quantum efficiency (η_{ext}), and 5 V turn-on voltages are achieved, affording a 250% increase in luminance and ~50% reduction in turn-on voltage, as compared to NPB-based devices. In the second case, even more dramatic enhancement is observed (64 000 cd/m^2 luminance; 2.3% η_{ext}; turn-on voltages as low as 3.5 V). The importance of the anode−HTL material contact is further explored by replacing NPB with saturated hydrocarbon siloxane monolayers that covalently bind to the anode, without sacrificing device performance (30 000 cd/m^2 luminance; 2.0% η_{ext}; 4.0 V turn-on voltage). These results suggest new strategies for developing OLED hole transporting structures.

1. Introduction

The past decade has witnessed the emergence of organic light-emitting diodes (OLEDs) as a practical display technology due to distinctive attractions such as low materials costs, self-emission, efficient and broad color tunability, compatibility with CMOS technology, and amenability to large-scale production.[1−5] Improving OLED electroluminescent characteristics has been the focus of an extensive worldwide research effort that has

led to appreciable fundamental understanding of the physical and chemical aspects of molecular solid-state electroluminescence (EL) and prototype devices with impressive performance.[6−13] The mechanism of emission in OLEDs is now reasonably well understood and involves injection of electrons and holes from the cathode and anode, respectively, under application of an electric field. Some fraction of the electron−hole pairs recombine to form excitons, which in turn radiatively

[†] Department of Chemistry and the Materials Research Center, Northwestern University.

[‡] Department of Physics and Astronomy and the Materials Research Center, Northwestern University.

[§] University of Arizona.

(1) For recent reviews of this subject, see: Veinot, J. G. C.; Marks, T. J. *Acc. Chem. Res.*, in press.
(2) Chen, C.-T. *Chem. Mater.* **2004**, *16*, 4389−4400.
(3) Nalwa, H. S. In *Handbook of Advanced Electronic and Photonic Materials and Devices*; Nalwa, H. S., Ed.; Academic: San Diego, CA, 2001; Vol. 10, pp 1−51.
(4) Mitschke, U.; Bauerle, P. *J. Mater. Chem.* **2000**, *10*, 1471−1507.
(5) Shim, H.-K.; Jin, J.-I. *Adv. Polym. Sci.* **2002**, *158*, 193−243.

(6) Niu, Y. H.; Hou, Q.; Cao, Y. *Appl. Phys. Lett.* **2003**, *82*, 2163−2165.
(7) Duan, J. P.; Sun, P. P.; Cheng, C. H. *Adv. Mater.* **2003**, *15*, 224−227.
(8) Mller, C. D.; Falcou, A.; Reckefuss, N.; Rojahn, M.; Wiederhirn, V.; Rudati, P.; Frohne, H.; Nuyken, O.; Becker, H.; Meerholz, K. *Nature* **2003**, *421*, 829−833.
(9) Niu, Y. H.; Yang, W.; Cao, Y. *Appl. Phys. Lett.* **2002**, *81*, 2884−2886.
(10) Herguch, P.; Jiang, X. Z.; Liu, M. S.; Jen, A. K. Y. *Macromolecules* **2002**, *35*, 6094−6100.
(11) Lo, S. C.; Male, N. A. H.; Markham, J. P. J.; Magennis, S. W.; Burn, P. L.; Salata, O. V.; Samuel, I. D. W. *Adv. Mater.* **2002**, *14*, 975−977.
(12) Huang, Q. L.; Cui, J.; Veinot, J. G. C.; Yan, H.; Marks, T. J. *Appl. Phys. Lett.* **2003**, *82*, 331−333.
(13) D'Andrade, B. W.; Baldo, M. A.; Adachi, C.; Brooks, J.; Thompson, M. E.; Forrest, S. R. *Appl. Phys. Lett.* **2001**, *79*, 1045−1047.
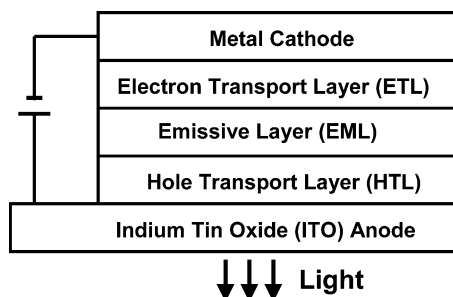
Figure 1. Cross-section of a typical multilayer OLED structure.

decay to ground states and emit light.[4] Sophisticated multilayer structures incorporating specifically tailored hole transport layers (HTLs), emissive layers (EMLs), and electron transport layers (ETLs) sandwiched between the two electrodes have been developed and generally exhibit superior device performance versus single-layer counterparts (Figure 1). To date, much effort has been devoted to developing new HTL materials to fulfill criteria such as substantial hole mobility, good energy level matching with anodes and EMLs (low hole injection barriers from the anode to the HTL and from the HTL to the EML; large electron injection barrier from the EML to the HTL), good thermal properties (stability; T_g), low optical absorption in the visible region, and smooth, amorphous film-forming morphology.[14−22]

To date, triarylamines have proven to be one of the most efficient classes of HTL molecules according to the above criteria, with 1,4-bis(phenyl-*m*-tolylamino)biphenyl (TPD, Scheme 1) an archetypical example. However, TPD has a low glass transition temperature (T_g = 65 °C) and tends to crystallize at elevated temperatures, disrupting the amorphous nature of the HTL and causing device degradation.[23] Therefore, one major focus in developing HTL materials is to improve the poor thermal stability of TPD by synthesizing small molecule TPD analogues with higher T_g parameters and/or by incorporating a triarylamine hole transport motif into a polymer chain.[20,24,25] In this regard, 1,4-bis(1-naphthylphenylamino)biphenyl (NPB, Scheme 1) is a TPD analogue with a higher T_g and has been widely used as a TPD replacement.[26] However, most of the effort in this direction has not led to significant device performance improvements over TPD-based OLEDs. In contrast, increasing evidence indicates that the anode (usually tin-doped

indium oxide, ITO)−HTL interface is crucial to hole injection in a common scenario where ITO−HTL contact rather than HTL bulk mobility limits charge injection.[27−31] A variety of interfacial engineering approaches have been applied to the anode−HTL junction,[32−37] including introduction of π-conjugated polymers,[38] copper phthalocyanine,[26,39,40] organic acids,[41] a thin layer of platinum,[28] self-assembled polar molecules[30,42] or siloxanes,[31,43] and plasma treatment of the ITO surface.[44] All of these approaches have effects on hole injection and yield varying degrees of improved device performance in terms of turn-on voltage, luminance, stability, and/or quantum efficiency. However, in general, the interlayers employed in these approaches cannot replace conventional triarylamine HTLs to yield high-performance OLEDs. Note that designing new HTL materials specifically targeting anode−HTL interfacial contact has largely been ignored.[14,15,45]

In this contribution, we present a full discussion of our efforts to design, synthesize, implement, and understand the consequences of hole transporting materials as OLED HTLs which achieve covalent ITO anode−HTL bonding (Scheme 2).[46] Followed by deposition of a conventional EML/ETL (tris(8-hydroxyquinolato)aluminum(III) (Alq, Scheme 1), this approach affords OLEDs with superior performance versus devices relying on simple ITO−NPB interfaces. For TPD-Si$_2$ functionalized anodes, luminances as high as 36 000 cd/m^2 with turn-on voltages as low as 5.0 V are achieved, 2.5× brighter and 4 V lower, respectively, than for analogous NPB-based devices. Also, a current efficiency of ~6 cd/A, equivalent to ~1.6% external forward quantum efficiency, is achieved at 12 V. We also show that the same approach can be applied as covalently bonded ITO anode−NPB interlayers, resulting in OLEDs with more impressive performance (64 000 cd/m^2 luminance; 8 cd/A

(14) Ren, X.; Alleyne, B. D.; Djurovich, P. I.; Adachi, C.; Tsyba, I.; Bau, R.; Thompson, M. E. *Inorg. Chem.* **2004**, *43*, 1697−1707.
(15) Hreha, R. D.; George, C. P.; Haldi, A.; Domercq, B.; Malagoli, M.; Barlow, S.; Bredas, J.-l.; Kippelen, B.; Marder, S. R. *Adv. Funct. Mater.* **2003**, *13*, 967−973.
(16) Gong, X.; Moses, D.; Heeger, A. J.; Liu, S.; Jen, A. K. Y. *Appl. Phys. Lett.* **2003**, *83*, 183−185.
(17) Ma, C.-Q.; Zhang, L.-Q.; Zhou, J.-H.; Wang, X.-S.; Zhang, B.-W.; Cao, Y.; Bugnon, P.; Schaer, M.; Nuesch, F.; Zhang, D.-Q.; Qiu, Y. *Chin. J. Chem.* **2002**, *20*, 929−932.
(18) Fujikawa, H.; Ishii, M.; Tokito, I.; Taga, Y. *Mater. Res. Soc. Symp. Proc.* **2001**, *621*, Q3.4.1−Q3.4.11.
(19) Liu, S.; Jiang, X.; Ma, H.; Liu, M. S.; Jen, A. K. Y. *Macromolecules* **2000**, *33*, 3514−3517.
(20) Koene, B. E.; Loy, D. E.; Thompson, M. E. *Chem. Mater.* **1998**, *10*, 2235−2250.
(21) Thayumanavan, S.; Barlow, S.; Marder, S. R. *Chem. Mater.* **1997**, *9*, 3231−3235.
(22) Tang, C. W.; VanSlyke, S. A. *Appl. Phys. Lett.* **1987**, *51*, 913−915.
(23) Adachi, C.; Tsutsui, T.; Saito, S. *Appl. Phys. Lett.* **1990**, *56*, 799−801.
(24) Santerre, F.; Bedja, I.; Dodelet, J. P.; Sun, Y.; Lu, J.; Hay, A. S.; D'Iorio, M. *Chem. Mater.* **2001**, *13*, 1739−1745.
(25) Shirota, Y.; Okumoto, K.; Inada, H. *Synth. Met.* **2000**, *111−112*, 387−391.
(26) Van Slyke, S. A.; Chen, C. H.; Tang, C. W. *Appl. Phys. Lett.* **1996**, *69*, 2160−2162.

(27) Forsythe, E. W.; Abkowitz, M. A.; Gao, Y. *J. Phys. Chem. B* **2000**, *104*, 3948−3952.
(28) Shen, Y.; Jacobs, D. B.; Malliaras, G. G.; Koley, G.; Spencer, M. G.; Ioannidis, A. *Adv. Mater.* **2001**, *13*, 1234−1238.
(29) Nesch, F.; Forsythe, E. W.; Le, Q. T.; Gao, Y.; Rothberg, L. J. *J. Appl. Phys.* **2000**, *87*, 7973−7980.
(30) Appleyard, S. F. J.; Day, S. R.; Pickford, R. D.; Willis, M. R. *J. Mater. Chem.* **2000**, *10*, 169−173.
(31) Malinsky, J. E.; Jabbour, G. E.; Shaheen, S. E.; Anderson, J. D.; Richter, A. G.; Marks, T. J.; Armstrong, N. R.; Kippelen, B.; Dutta, P.; Peyghambarian, N. *Adv. Mater.* **1999**, *11*, 227−231.
(32) Zuppiroli, L.; Si-Ahmed, L.; Kamars, K.; Nesch, F.; Bussac, M. N.; Ades, D.; Siove, A.; Moons, E.; Grtzel, M. *Eur. Phys. J. B* **1999**, *11*, 505−512.
(33) Ho, P. K. H.; Granstrom, M.; Friend, R. H.; Greenham, N. C. *Adv. Mater.* **1998**, *10*, 769−771.
(34) Nesch, F.; Rtzinger, F.; Si-Ahmed, L.; Zuppiroli, L. *Chem. Phys. Lett.* **1998**, *288*, 861−867.
(35) Morgado, J.; Charas, A.; Barbagallo, N.; Alcacer, L.; Matos, M.; Cacialli, F. *Macromol. Symp.* **2004**, *212*, 381−386.
(36) Hatton, R. A.; Willis, M. R.; Chesters, M. A.; Rutten, F. J. M.; Briggs, D. *J. Mater. Chem.* **2003**, *13*, 38−43.
(37) Campbell, I. H.; Kress, J. D.; Martin, R. L.; Smith, D. L.; Barashkov, N. N.; Ferraris, J. P. *Appl. Phys. Lett.* **1997**, *71*, 3528−3530.
(38) Gross, M.; Muller, D.; Nothofer, H.; Scherf, U.; Neher, D.; Brauchle, C.; Meerholz, K. *Nature* **2000**, *405*, 661−665.
(39) Tadayyon, S. M.; Grandin, H. M.; Griffiths, K.; Norton, P. R.; Aziz, H.; Popovic, Z. D. *Org. Electron.* **2004**, *5*, 157−166.
(40) Mori, T.; Mitsuoka, T.; Ishii, M.; Fujikawa, H.; Taga, Y. *Appl. Phys. Lett.* **2002**, *80*, 3895−3897.
(41) Nesch, F.; Forsythe, E. W.; Le, Q. T.; Gao, Y.; Rothberg, L. J. *J. Appl. Phys.* **2000**, *87*, 7973−7976.
(42) Ganzorig, C.; Kwak, K. J.; Yagi, K.; Fujihira, M. *Appl. Phys. Lett.* **2001**, *79*, 272−274.
(43) Cui, J.; Huang, Q.; Wang, Q.; Marks, T. J. *Langmuir* **2001**, *17*, 2051−2054.
(44) Milliron, D. J.; Hill, I. G.; Shen, C.; Kahn, A.; Schwartz, J. *J. Appl. Phys.* **2000**, *87*, 572−576.
(45) Adachi, C.; Nagai, K.; Tamoto, N. *Appl. Phys. Lett.* **1995**, *66*, 2679−2681.
(46) Portions of this work were previously communicated in part. Huang, Q.; Evmenenko, G.; Dutta, P.; Marks, T. J. *J. Am. Chem. Soc.* **2003**, *125*, 14704−14705. Cui, J.; Huang, Q.; Veinot, J. C. G.; Yan, H.; Wang, Q.; Hutchison, G. R.; Richter, A. G.; Evmenenko, G.; Dutta, P.; Marks, T. J. *Langmuir* **2002**, *18*, 9958−9970.

Scheme 1. Structures of Multilayer OLED Constituent Materials: TPD, NPB, and PEDOT(HTL), Alq (EML/ETL), DIQA(EML Dopant), and BCP (ETL)
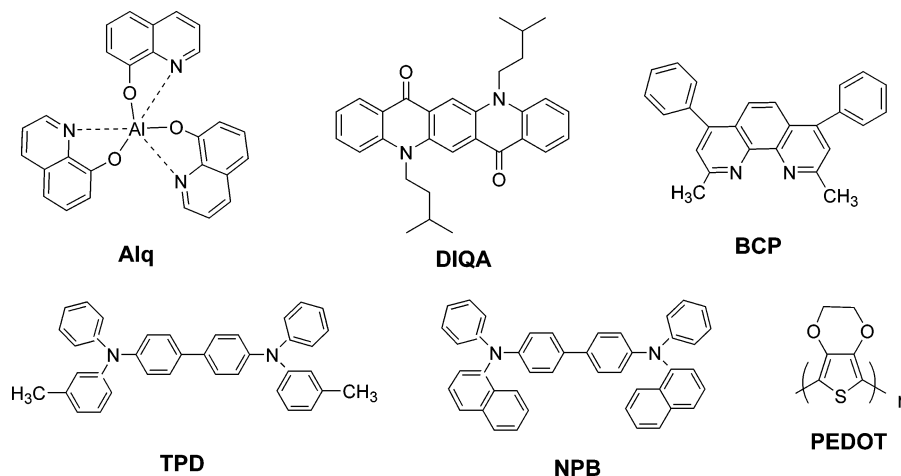
Scheme 2. Chemical Structures of the Organosiloxanes Used as HTLs and ITO Anode Modification Layers
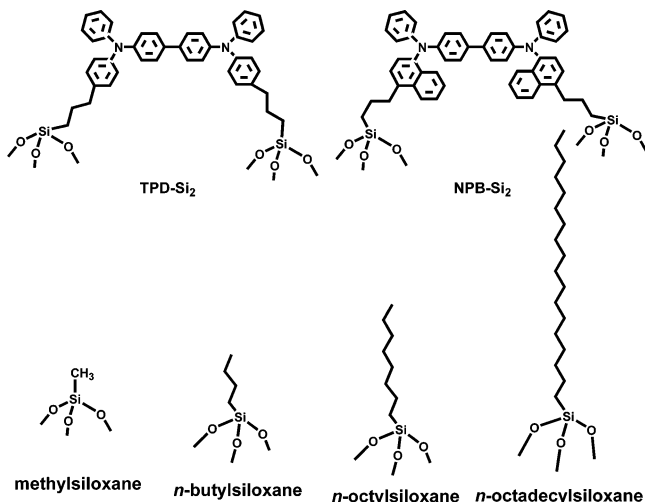
current efficiency at 10 V; turn-on voltages as low as 3.5 V). These anode functionalization processes are expected to significantly modify anode−HTL interfacial properties,[47] and here we discuss how these modifications translate into modified OLED EL device response. We also present here evidence that simple saturated hydrocarbon self-assembled monolayers (SAMs; Scheme 2) can function as HTLs and ITO−NPB interlayers, affording a better understanding of silane-anode modification effects. Devices with luminances as high as 30 000 cd/m² and current efficiencies of ~7 cd/A, equivalent to ~2% external forward quantum efficiency, at 7.0 V can be achieved. Taken together, these results require some reassessment of current HTL structure−function models.

2. Experimental Section

Materials and Methods. ITO glass sheets (20 Ω/□, rms roughness = 2.5 nm) were purchased from Colorado Concept Coating. All chemical reagents were used as received unless otherwise indicated. All manipulations of air/moisture-sensitive materials were carried out on a dual-manifold Schlenk line or in a nitrogen-filled glovebox. Ether and THF were distilled before use from sodium/benzophenone ketyl. Methylene chloride was distilled before use from calcium hydride. Toluene was dried using activated alumina and Q5 columns and tested with benzyphenone ketyl in ether solution. TPD and Alq were purchased

from Sigma-Aldrich and purified via vacuum gradient sublimation. The OLED component, 2,9-dimethyl-4,7-diphenyl-1,10-phenanthroline (BCP, Scheme 1), was purchased from Fluka and purified via vacuum gradient sublimation. NPB was synthesized according to the literature[20] and was purified by recrystallization followed by vacuum gradient sublimation. *N,N′*-Di(3-heptyl)quinacridone (DIQA, Scheme 1) was synthesized and purified according to the literature.[48] NMR spectra were obtained on Varian VXR-400 or 500 MHz NMR instruments. MS analyses were conducted on a Micromass Quattro II Triple Quadrupole HPLC/MS/MS mass spectrometer. Elemental analyses were carried out by Midwest Microlabs. Cyclic voltammetry was performed with a BAS 100 electrochemical workstation (SAM-coated ITO with ~1 cm² area working electrodes, Ag wire pseudo-reference electrode, Pt wire counter electrode, 0.1 M TBAHFP in anhydrous MeCN supporting electrolyte, and 0.001 M ferrocene as the internal pinhole probe; scan rate = 0.1 V/s). TBAHFP was recrystallized from an ethyl acetate/hexanes mixture and dried in vacuo at 100 °C for 10 h. Ferrocene was purchased from Sigma-Aldrich and purified via vacuum gradient sublimation. IR spectra were obtained on a Bio-Rad FTS-40 FTIR spectrometer. AFM images were obtained on a Nanoscope III AFM under ambient conditions in the contact mode with Si₃N₄ cantilevers. Specular X-ray reflectivity experiments on coated single-crystal Si (111) or Si (100) substrates were performed on the Naval Research Laboratory X23B beamline at the National Synchrotron Light Source. Data were acquired and analyzed as described previously.[46] The thickness of spin-cast films was measured with a Tencor P-10 profilometer. Ultraviolet photoelectron spectroscopy (UPS) experiments on TPD-Si₂ and NPB-Si₂ SAM-coated ITO substrates were carried out at the University of Arizona using the 21.2 eV He (I) source (Omicron H15-13) of a Kratos Axis-165 Ultra photoelectron spectrometer. HOMO values were estimated from the median energy of the clearly defined photoionization peak, while IP values were estimated from the extrapolation of the high kinetic energy edge of that peak to zero intensity.

Synthesis of 4,4′-Bis[(*p*-bromophenyl)phenylamino)]biphenyl (1). To a toluene solution (50 mL) of tris(dibenzyldeneacetone)dipalladium (0.55 g, 0.60 mmol) and bis(diphenylphosphino)ferrocene (0.50 g, 0.90 mmol) was added 1,4-dibromobenzene (18.9 g, 0.0800 mol) at 25 °C. Following stirring under an N₂ atmosphere for 10 min, sodium *tert*-butoxide (4.8 g, 0.050 mol) and *N,N′*-diphenylbenzidine (6.8 g, 0.020 mol) were added. The reaction mixture was then stirred at 90 °C for 12 h, followed by cooling to 25 °C. The reaction mixture was then poured into water, and the organic and aqueous layers were separated. The aqueous layer was extracted with toluene (3 × 100 mL), and the

(47) Cahen, D.; Hodes, G. *Adv. Mater.* **2002**, *14*, 789−798.
(48) Shaheen, S. E.; Kippelen, B.; Peyghambarian, N.; Wang, J. F.; Anderson, J. D.; Mash, E. A.; Lee, P. A.; Armstrong, N. R.; Kawabe, Y. *J. Appl. Phys.* **1999**, *85*, 7939−7945.

resulting extracts were combined with the original organic layer. The solvent was removed in vacuo giving a crude product which was purified by chromatography on a silica gel column (6:1 hexane:ethylene chloride eluent) to yield pure **1** as a colorless solid (6.9 g) in 50% yield. ^{1}H NMR (CDCl$_3$): δ 6.99 (d, $J = 8.8$ Hz, 4H), 7.02−7.16 (m, 10H), 7.28 (t, $J = 7.6$ Hz, 4H), 7.34 (d, $J = 8.8$ Hz, 4H), 7.45 (d, $J = 8.4$ Hz, 4H).

Synthesis of 4,4′-Bis[(p-allylphenyl)phenylamino]biphenyl (2). Using standard Schlenk techniques, 1.6 mL (3.5 mmol) of *n*-butyllithium(2.5 M in hexanes) was added dropwise under inert atmosphere to an ether solution (10 mL) of **1** (1.02 g, 1.58 mmol) while maintaining the temperature at 25 °C. The mixture was stirred for 2 h, after which time CuI (0.76 g, 4.0 mmol) was added. Upon cooling the reaction mixture to 0 °C, allyl bromide (0.60 g, 5.0 mmol) was added in one portion, and the mixture was stirred for 14 h, followed by quenching with saturated aqueous NH$_4$Cl solution (100 mL) and extraction with ether (3 × 100 mL). The combined ether extracts were washed with water (2 × 100 mL) and brine (2 × 100 mL), and dried over anhydrous Na$_2$SO$_4$. Filtration and removal of solvent in vacuo afforded a yellow oil, which was further purified by chromatography on a silica gel column (4:1 hexane:methylene chloride) to yield 0.63 g of pure **2** as a colorless solid. Yield, 70%. ^{1}H NMR (CDCl$_3$): δ 3.40 (d, $J = 10$ Hz, 4H), 5.10−5.20 (m, 4H), 6.02 (m, 2H), 6.99−7.10 (m, 2H), 7.10−7.20 (m, 16H), 7.28 (t, $J = 7.6$ Hz, 4H), 7.46 (d, $J = 8.8$ Hz, 4H). Anal. Calcd for C$_{42}$H$_{36}$N$_2$: C, 88.68; H, 6.39; N, 5.23. Found: C, 87.50; H, 6.35; N, 4.93.

Synthesis of 4,4′-Bis[(p-trichlorosilylpropylphenyl)phenylamino]-biphenyl (TPD-Si$_2$, 3). Under inert atmosphere at 25 °C, a grain of H$_2$PtCl$_6$·*n*H$_2$O, followed by HSiCl$_3$ (0.73 g, 5.5 mmol), was added to a CH$_2$Cl$_2$ solution (30 mL) of **2** (0.32 g, 0.55 mol), and the reaction mixture was stirred at 30 °C for 4 h. Removal of the solvent in vacuo yielded a dark-yellow oil, which was triturated with a mixture of 50 mL of pentane and 10 mL of toluene to yield a solid that was removed by filtration. The filtrate was concentrated in vacuo to yield **3** as a viscous, pale-yellow oil. Yield, 98%. ^{1}H NMR (CDCl$_3$): δ 1.45 (t, $J = 7$ Hz, 4H), 1.90 (t, $J = 7$ Hz, 4H), 2.70 (brs, 4H), 6.80−7.80 (m, 26H). Anal. Calcd for C$_{42}$H$_{38}$Cl$_6$N$_2$Si$_2$: C, 60.07; H, 4.57. Found: C, 60.52; H, 4.87.

Synthesis of N,N′-Bis(p-bromonaphthalen-1-yl)-N,N′-diphenyl-biphenyl-4,4′-diamine (4). To a toluene solution (50 mL) of tris-(dibenzylideneacetone)dipalladium (0.048 g, 0.052 mmol) and bis-(diphenylphosphino)ferrocene (0.044 g, 0.079 mmol) was added 1,4-dibromonaphathelene (1.0 g, 3.5 mmol) at 25 °C. Following stirring under an N$_2$ atmosphere for 10 min, sodium *tert*-butoxide (0.34 g, 3.5 mmol) and N,N′-diphenylbenzidine (0.47 g, 1.4 mmol, purified by sublimation) were added. The reaction mixture was stirred at 90 °C for 22 h, followed by cooling to 25 °C. The reaction mixture was then poured into water, and the organic and aqueous layers were separated. The aqueous layer was extracted with toluene (3 × 100 mL), and the resulting extracts were combined with the original organic layer. The solvent was removed in vacuo giving a crude product that was purified by chromatography on a silica gel column (6:1 hexane:methylene chloride eluent) to yield pure **4** as a colorless solid (0.20 g) in 20% yield. ^{1}H NMR (CDCl$_3$): δ 6.96−7.05 (m, 10H), 7.19−7.23 (m, 6H), 7.36−7.42 (m, 4H), 7.57 (t, $J = 8.5$ Hz, 4H), 7.77 (d, $J = 9.5$ Hz, 2H), 7.98 (d, $J = 10.5$ Hz, 2H), 8.27 (d, $J = 10.5$ Hz, 2H).

Synthesis of N,N′-Bis(p-allylnaphthalen-1-yl)-N,N′-diphenyl-bi-phenyl-4,4′-diamine (5). To a stirring, anhydrous THF solution (10 mL) of **4** (0.10 g, 0.13 mmol) under inert atmosphere was added dropwise at −78 °C *n*-butyllithium (1.6 M in hexanes, 0.17 mL, 0.27 mmol), and the mixture was stirred for 15 min. Copper iodide(I) (0.051 g, 0.27 mmol) was then added. After the mixture was stirred for 5 min, allyl bromide (0.07 g, 0.54 mmol) was added in one portion. The solution was gradually warmed to 25 °C and stirred for 2 h, after which time it was quenched with 100 mL of saturated aqueous NH$_4$$^+Cl^-$ solution, followed by extraction with ether (3 × 100 mL). The combined

ether extracts were washed with water (2 × 100 mL) and brine (2 × 100 mL), and dried over anhydrous Na$_2$SO$_4$. Following filtration, the solvent was removed in a vacuum to yield an oil. Chromatography on silica gel with hexane:methylene chloride (10:1) afforded 0.070 g of **5** as a colorless solid. Yield, 80%. ^{1}H NMR (CDCl$_3$): δ 3.90 (d, $J = 4.5$ Hz, 4H), 5.17−5.20 (m, 4H), 6.20 (m, 2H), 6.95 (t, $J = 7.5$ Hz, 2H), 7.06−7.10 (m, 10H), 7.21−7.24 (m, 4H), 7.30 (d, $J = 7.5$ Hz, 2H), 7.37−7.40 (m, 8H), 7.50−7.53 (m, 2H), 8.04 (d, $J = 8.0$ Hz, 2H), 8.09 (d, $J = 9.0$ Hz, 2H). MS (*m/z*): 669.2 [M, 100]. Anal. Calcd for C$_{50}$H$_{40}$N$_2$: C, 89.77; H, 6.04; N, 4.19. Found: C, 89.54; H, 6.04; N, 4.21.
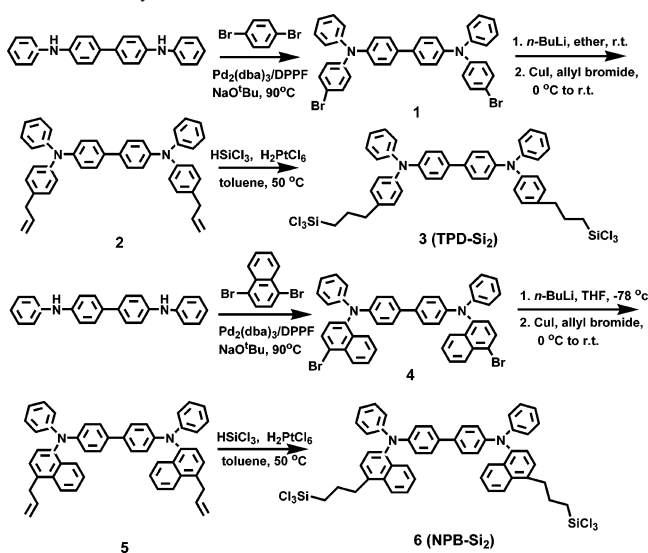
Synthesis of N,N′-Bis(p-trichlorosilylpropyl)-naphthalen-1-yl)-N,N′-diphenyl-biphenyl-4,4′-diamine (NPB-Si$_2$, 6). To a solution of **5** (0.040 g, 0.060 mmol) in 25 mL of dry toluene at 25 °C under inert atmosphere was added H$_2$PtCl$_6$·*n*H$_2$O (0.001 g), followed by trichlorosilane (0.060 mL, 0.60 mmol). The reaction solution was warmed to 50 °C and monitored by NMR until the completion of reaction. Removal of the solvent in a vacuum yielded an oil. Next, 20 mL of dry toluene was added to the residue and the resulting solution was filtered into a Schlenk flask by cannula. The filtrate was concentrated under vacuum to give **6** as a pale-yellow oil. Yield, 98%. ^{1}H NMR (CDCl$_3$): δ 1.70 (t, $J = 6.0$ Hz, 4H), 2.10 (t, $J = 7$ Hz, 4H), 3.21 (t, $J = 7$ Hz, 4H), 6.94 (m, 2H), 7.03−7.07 (m, 10H), 7.19−7.22 (m, 4H), 7.33−7.40 (m, 8H), 7.50−7.53 (m, 2H), 7.54 (d, $J = 8.0$ Hz, 2H), 7.72 (d, $J = 9.0$ Hz, 2H), 8.04 (d, $J = 9.0$ Hz, 2H). Anal. Calcd for C$_{50}$H$_{42}$Cl$_6$N$_2$Si$_2$: C, 63.90; H, 4.50; N, 2.98. Found: C, 63.54; H, 4.04; N, 2.90.

Self-Assembly of TPD-Si$_2$ and NPB-Si$_2$ on ITO Substrates. ITO substrates were cleaned in an ultrasonic detergent bath, followed by methanol, 2-propanol, and finally acetone. The substrates were subsequently treated in an oxygen plasma cleaner for 1 min to remove any residual organic contaminants. Following strict Schlenk protocol, clean ITO substrates were immersed in a 1.0 mM dry toluene solution of TPD-Si$_2$ or NPB-Si$_2$, respectively. After heating at ∼80 °C for 1 h, the toluene solution was removed by cannula and the substrates were rinsed with dry toluene (2 × 50 mL) and wet acetone, followed by transferring to a 120 °C oven for 1 h to expedite cross-linking. Longer thermal curing yields films with similar properties, and the coating procedure has negligible effects on the measured sheet resistance of the underlying ITO.

Self-Assembly of TPD-Si$_2$ and NPB-Si$_2$ on Silicon Substrates. Silicon (111) or (100) substrates (Semiconductor Processing Co.) were subjected to a cleaning procedure as follows: immersion in "piranha" solution (concentrated H$_2$SO$_4$:30% H$_2$O$_2$; 70:30 v/v) at 80 °C for 1 h. After being cooled to room temperature, substrates were rinsed repeatedly with deionized (DI) water followed by an RCA-type cleaning protocol (H$_2$O:30% H$_2$O$_2$:NH$_3$; 5:1:1 v/v/v; sonicated at room temperature for 40 min). The substrates were finally rinsed with copious amounts of DI water, heated to 125 °C for 15 min, and dried in vacuo. TPD-Si$_2$ and NPB-Si$_2$ were then self-assembled onto the clean silicon substrates following the procedure described above for ITO substrates.

Spin-Casting TPD-Si$_2$ and NPB-Si$_2$ on ITO Substrates. Dry toluene solutions of TPD-Si$_2$ or NPB-Si$_2$ (10 mg/mL) were spin-coated onto clean ITO surfaces at 2 krpm in air, followed by curing in a vacuum oven at 110 °C for 1 h.

Fabrication of OLED Devices. All OLED devices were fabricated on bare ITO substrates that were treated with solvents and an oxygen plasma, as described previously, or on TPD-Si$_2$/NPB-Si$_2$ modified ITO substrates. The substrates were loaded into a bell jar deposition chamber housed in a nitrogen-filled glovebox. A typical deposition procedure is as follows: at 1×10^{-6} Torr, a 20 nm layer of NPB was first deposited, followed by 60 nm of Alq doped with 1% DIQA. Both organic layers were grown at a deposition rate of 2−3 Å/s. Another 20 nm thick layer of BCP was then deposited, followed by thermally evaporating 1 nm thick Li. Finally, a 100 nm thick Al cathode was deposited through a shadow mask. This metallic layer was patterned via a shadow

Scheme 3. Synthesis of TPD-Si$_2$ and NPB-Si$_2$

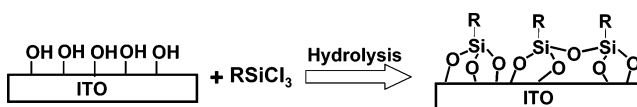**Scheme 4.** Scheme for ITO Surface Modified by Covalently Bound HTL Materials

mask to give four devices, each with an area of 0.10 cm^2. OLED device characterization was carried out with a computer-controlled Keithley 2400 source meter and IL 1700 research radiometer equipped with a calibrated silicon photodetector at 25 °C under ambient atmosphere. External quantum efficiency was estimated from current density versus voltage and luminance versus current density characteristics.

Fabrication of Hole-Only Devices. All hole-only devices were fabricated on bare ITO substrates that were treated with solvents and an oxygen plasma, as described previously, or on TPD-Si$_2$/NPB-Si$_2$ modified ITO substrates. The substrates were loaded into a bell jar deposition chamber housed within a nitrogen-filled glovebox. At a base pressure of 1×10^{-6} Torr, NPB (400 nm) was vapor deposited at a rate of ~3 Å/s, followed by sputter-coating of a 6 nm of Au layer through the same shadow mask employed for OLED fabrication described above. Single-carrier device assembly was subsequently completed with the masked thermal vapor deposition of Al (150 nm). Device behavior was evaluated using the computer-controlled Keithley 2400 sourcemeter.

3. Results

In Section 3.1, we report the deposition and characterization of TPD-Si$_2$ and NPB-Si$_2$ on ITO or Si substrates. In Section 3.2, spin-coated or self-assembled TPD-Si$_2$ and NPB-Si$_2$ layers replace the conventional vapor-deposited NPB layer in Alq-based OLEDs. Their current/luminous functions as new types of covalently bonded HTLs are described. Alternatively, TPD-Si$_2$ and NPB-Si$_2$ are used as ITO anode−NPB interlayers, and the effect on OLED EL response is analyzed here. In Section 3.3, alkylsiloxane SAMs are employed as HTLs and ITO−NPB interlayers, and the effect on device performance is compared to that of the above triarylaminesiloxanes.

3.1. Deposition and Characterization of TPD-Si$_2$ and NPB-Si$_2$ on ITO or Silicon Substrates. The synthetic pathways to TPD-Si$_2$ and NPB-Si$_2$ are summarized in Scheme 3, while detailed procedures and characterization data are presented in the Experimental Section. Utilizing a self-limiting, solution-based chemisorption process, TPD-Si$_2$ and NPB-Si$_2$ are self-assembled onto hydrophilic ITO substrate surfaces with nano-precise control in thickness. As illustrated in Scheme 4, clean ITO-coated glass or single-crystal silicon surfaces possess hydroxyl functionalities and adsorbed water, which are reactive toward chlorosilanes, thereby affording covalent binding of the

silanes to the surface.[49−52] Further exposure to air and moisture in the following wet acetone rinse in air hydrolyzes any unreacted trichlorosilyl groups. Thermal curing facilitates the formation of cross-linked siloxane networks, resulting in a thin layer consisting of hole transporting motifs covalently anchored to the ITO or Si surface. At completion of the silane condensation, chlorine concentrations in the film are below XPS detection limits.[53,54] The microstructural characterization of these layers is presented below. Spin-casting TPD-Si$_2$ and NPB-Si$_2$ from hydrocarbon solutions onto ITO or Si substrates affords thicker (~40 nm) films on these substrates, following chemistry similar to that described above, given that the spin-coating parameters such as solution concentration and spinning speed are carefully controlled (see Experimental Section for details).

Characterization of TPD-Si$_2$ and NPB-Si$_2$ Siloxane Films by Specular X-ray Reflectivity Measurements. Specular X-ray reflectivity (XRR) measurements were performed upon the films deposited on cleaned single-crystal Si(111) or Si (100) surfaces, using the self-assembly procedure discussed above. Fitting of the X-ray reflectivity data, normalized to the Fresnel reflectivity, to a physically reasonable model provides details of the film thickness, smoothness, interfacial abruptness, and density. In general, the reflectivity can be expressed in terms of the average electron density by eqs 1 and 2,[55]

$$R(k_z) = R_F(k_z)|\Phi(k_z)|^2 \tag{1}$$

$$\Phi(k_z) = \int \frac{1}{\rho_\infty} \frac{d\langle \rho \rangle}{dz} e^{ik_z z} \, dz \tag{2}$$

where R_F is the theoretical Fresnel reflectivity for a smooth interface, k_z is the momentum transferred ($k_z = 4\pi/\lambda \sin \theta$), $d\langle \rho \rangle/dz$ is the derivative of the electron density along the surface normal direction, averaged over the in-plane coherence length of the X-rays, and ρ_∞ is the electron density of the substrate (Si). By fitting the XRR data for the self-assembled TPD-Si$_2$ and NPB-Si$_2$ films on Si, the thickness, electron density, and roughness were determined. These data are compiled in Table 1.

Characterization of Self-Assembled TPD-Si$_2$ and NPB-Si$_2$ Monolayers by Ultraviolet Photoelectron Spectroscopy (UPS). UPS measurements were conducted on ITO surfaces covered with TPD-Si$_2$ and NPB-Si$_2$ SAMs. The bare ITO surface, which had been Ar$^+$-sputtered in vacuo, is used

(49) Ulman, A. *Chem. Rev.* **1996**, *96*, 1533−1554.
(50) Jeon, N. L.; Nuzzo, R. G.; Xia, Y.; Mrksich, M.; Whitesides, G. M. *Langmuir* **1995**, *11*, 3024−3026.
(51) Ulman, A. *Thin Solid Films* **1996**, *273*, 48−53.
(52) Woodward, J. T.; Ulman, A.; Schwartz, D. K. *Langmuir* **1996**, *12*, 3626−3629.
(53) Donley, C.; Dunphy, D.; Paine, D.; Carter, C.; Nebesny, K.; Lee, P.; Alloway, D.; Armstrong, N. R. *Langmuir* **2002**, *18*, 450−457.
(54) Malinsky, J. E.; Veinot, J. C. G.; Jabbour, G. E.; Shaheen, S. E.; Anderson, J. D.; Lee, P.; Richter, A. G.; Burin, A. L.; Ratner, M. A.; Marks, T. J.; Armstrong, N. R.; Kippelen, B.; Dutta, P.; Peyghambarian, N. *Chem. Mater.* **2001**, *14*, 3054−3065.
(55) Richter, A. G.; Yu, C. J.; Datta, A.; Kmetko, J.; Dutta, P. *Phys. Rev. E* **2000**, *61*, 607−615.

Table 1. XRR-Derived Electron Density, Roughness, and Thickness Data for Self-Assembled TPD-Si$_2$ and NPB-Si$_2$ Monolayers on Si (100) Substrates

monolayer	electron density (e Å^{-3})	roughness (Å)	thickness (Å)
TPD-Si$_2$	0.32−0.35	7.8 ± 0.2	17.8 ± 0.2
NPB-Si$_2$	0.45−0.47	4.1 ± 0.2	14.1 ± 0.2

Table 2. UPS Measured Ionization Potential, Highest Occupied Molecular Orbital (HOMO) Energy, and Vacuum Level Shift for TPDSi$_2$ and NPBSi$_2$ Self-Assembled Monolayers on ITO Substrates

	ionization potential (eV)	HOMO (eV)	vacuum level shift (eV)
TPD-Si$_2$	5.2	6.1	±0.1
NPB-Si$_2$	5.4	6.1	−0.1

as reference for the low kinetic energy edge of the photoemission spectrum in the measurement. A 0.1 eV shift in the low kinetic energy edge of the photoemission spectrum obtained from the analysis of the SAM-covered ITO surface is observed for both TPD-Si$_2$ and NPB-Si$_2$, indicating interfacial dipole formation.[56] The sign of the vacuum level shift for the TPD-Si$_2$ SAMs is uncertain due to experimental errors. Estimates of the effective surface work function can be obtained from the measured width of the UV-photoemission spectrum, subtracted from the source energy, using the high and low kinetic energy edges of the photoemission spectra. The analysis shows nearly identical HOMO and IP values for TPD-Si$_2$ and NPB-Si$_2$ SAM modified ITO surfaces (5.2 and 5.4 eV, respectively, Table 2).

Characterization of TPD-Si$_2$ and NPB-Si$_2$ Siloxane Films by Atomic Force Microscopy. Contact mode AFM imaging was carried out on three spots randomly chosen on self-assembled or spin-cast TPD-Si$_2$ or NPB-Si$_2$ covered ITO substrates, respectively. Uniform films with no evidence of cracks or pinholes were observed over a 5 × 5 μm scan area (Figure 2). The rms roughness is 1.39 and 3.18 nm, respectively, for TPD-Si$_2$ and NPB-Si$_2$ SAMs, and 0.79 and 3.43 nm, respectively, for spin-coated TPD-Si$_2$ and NPB-Si$_2$ films, as compared to bare ITO substrates with an rms roughness of 2.5 nm.
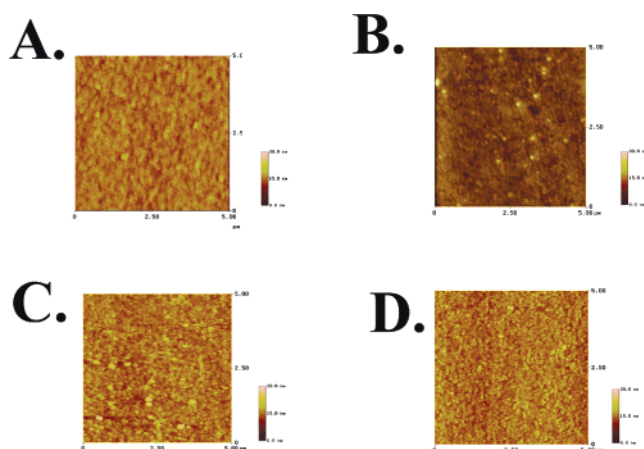
Figure 2. Tapping mode AFM images of self-assembled and spin-cast TPD-Si$_2$ and NPB-Si$_2$ films on ITO substrates. (A) TPD-Si$_2$ SAM on ITO. RMS roughness = 1.39 nm. (B) TPD-Si$_2$ spin coated film on ITO. RMS roughness = 0.79 nm. (C) NPB-Si$_2$ SAM on ITO. RMS roughness = 3.18 nm. (D) NPB-Si$_2$ spin coated film on ITO. RMS roughness = 3.43 nm.
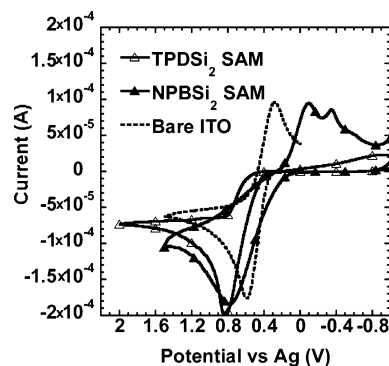
Figure 3. Cyclic voltammetry characteristics of self-assembled TPD-Si$_2$ and NPB-Si$_2$ monolayer films on an ITO electrode immersed in a ferrocene solution. Electrolyte: 0.1 M TBAHFP in anhydrous MeCN. Sweep speed: 0.1 V/s.

Characterization of TPD-Si$_2$ and NPB-Si$_2$ Siloxane Films by Cyclic Voltammetry. TPD-Si$_2$ and NPB-Si$_2$ SAM-coated ITO, silver wire, and Pt wire were used as the working electrode, reference electrode, and counter electrode, respectively, in 0.1 M acetonitrile solution of tetrabutylammonium hexafluorophosphate as the electrolyte without the ferrocene. Integration of the oxidation peak areas and assuming two electron oxidation/reduction events per molecular unit yields surface coverages of 2.5×10^{-10} mol/cm^2 (TPD-Si$_2$ SAM) and 2.2×10^{-10} mol/cm^2 (NPB-Si$_2$ SAM), respectively.[57] Analogously, a close-packed monolayer of ferrocene dicarboxylic acid absorbed on ITO yields 4.0×10^{-10} mol/cm^2 surface coverage.[53]

To examine the present HTL SAMs for pinholes over the entire ITO substrate area, cyclic voltammetry experiments using ferrocene as a redox probe were then carried out.[58] Here, TPD-Si$_2$ or NPB-Si$_2$ SAM-coated ITO substrates were used as working electrodes. Bare ITO substrates were used as references to calibrate the ferrocene redox potential for each measurement. It was observed that the ferrocene oxidation potential shifts from 0.59 V, as shown in Figure 3, when bare ITO substrates are used as working electrodes, to 0.84 and 0.77 V, respectively, for the TPD-Si$_2$ and NPB-Si$_2$ SAM-covered ITO substrates as working electrodes. It is expected that the pinhole-free films of TPD-Si$_2$ and NPB-Si$_2$ SAMs on ITO electrodes will block the oxidation of solution ferrocene, until potentials are reached where the bis-trarylamine groups are oxidized, providing sites for mediated oxidation of solution phase ferrocene.[59,60] For both TPD-Si$_2$ and NPB-Si$_2$ SAMs on ITO, the peak potential for oxidation of ferrocene is indeed shifted positively by ca. 0.2 V. The reduction of the ferricenium cation on the return sweep is partially blocked by the NPB-Si$_2$ layer, and more completely blocked by the TPD-Si$_2$ layer, suggesting that the latter SAM layer is somewhat more pinhole free.[61] The larger separations of ferrocene oxidative and reductive peak potentials at the SAM-coated ITO electrodes versus on the bare ITO ones

(56) Ishii, H.; Sugiyama, K.; Ito, E.; Seki, K. *Adv. Mater.* **1999**, *11*, 605−625.
(57) Murray, R. W. In *Molecular Design of Electrode Surfaces, Techniques of Chemistry*; Murray, R. W., Ed.; Wiley: New York, 1992; Vol. 22, pp 1−158.
(58) DuBois, C. J., Jr.; McCarley, R. L. *J. Electroanal. Chem.* **1998**, *454*, 99−105.
(59) Immoos, C. E.; Chou, J.; Bayachou, M.; Blair, E.; Greaves, J.; Farmer, P. J. *J. Am. Chem. Soc.* **2004**, *126*, 4934−4942.
(60) Nowall, W. B.; Kuhr, W. G. *Anal. Chem.* **1995**, *67*, 3583−3588.
(61) Inzelt, G. In *Electroanalytical Chemistry*; Bard, A. J., Rubenstein, I., Eds.; Marcel Dekker: New York, 1994; Vol. 18, pp 90−134.

(1.68 V, TPD-Si$_2$ SAM; 0.86 V, NPB-Si$_2$ SAM; 0.30 V, bare ITO) may also indicate that in the redox processes, counterion penetration and diffusion in the SAMs are retarded, presumably due to the densely packed, cross-linked SAM networks.[62−65] It is likely that TPD-Si$_2$, due to its smaller core triarylamine molecular volume, encounters less steric hindrance in the film-forming intermolecular cross-linking process as compared to NPB-Si$_2$, resulting in more densely packed films. The more distorted curve shape for the TPD-Si$_2$ SAM is presumably related to its more densely packed, cross-linked coverage and different π-system redox kinetics versus NPB-Si$_2$.

3.2. Self-Assembled and Spin-Cast TPD-Si$_2$ and NPB-Si$_2$ Films in OLEDs. Replacing NPB with TPD-Si$_2$ and NPB-Si$_2$ SAMs in OLEDs. Alq-based OLEDs having the structure ITO anode/HTL/Alq doped with DIQA/BCP doped with Li/Al were fabricated to study the function of TPD-Si$_2$ and NPB-Si$_2$ films as HTLs. Replacing vapor-deposited conventional 20 nm thick NPB HTLs with nanometer-scale thick SAMs of TPD-Si$_2$ or NPB-Si$_2$ in the above OLEDs was first investigated, and EL response data are shown in Figure 4. Note that the OLEDs exhibit greater luminance and, in some regimes, higher external quantum efficiencies when the conventional 20 nm thick HTL (NPB) is replaced with ~2 nm thick TPD-Si$_2$ and NPB-Si$_2$ SAMs. The maximum luminance is ~18 000 cd/m^2 (NPB-Si$_2$), ~17 000 cd/m^2 (TPD-Si$_2$), and ~14 000 cd/m^2 (NPB-only). Also, the NPB-Si$_2$ and TPD-Si$_2$ SAM-based OLEDs have lower turn-on and operating voltages. For instance, the operating voltage at 300 cd/m^2, a standard brightness for displays, is 8.0, 8.5, and 10.5 V for NPB-Si$_2$, TPD-Si$_2$, and NPB-only, respectively. However, the maximum external forward quantum efficiencies are 0.8% (NPB-Si$_2$), 0.75% (TPD-Si$_2$), and 1.87% (NPB-only). OLEDs without HTLs were also fabricated here as a comparison, and the dramatic effects on device performance induced by the SAMs are clearly evident (Figure 4).

Replacing Conventional HTLs with Spin-Cast TPD-Si$_2$ and NPB-Si$_2$ Films in OLEDs. TPD-Si$_2$ and NPB-Si$_2$ were spin-coated onto ITO substrates and thermally cured in a vacuum oven at 110 °C for 1 h, yielding films with a thickness of ~40 nm, as measured by profilometry, followed by vapor-deposition of Alq doped with DIQA, then BCP, Li, and Al. Again, replacing NPB with the cross-linked siloxane films results in higher luminance and external quantum efficiencies at identical bias (Figure 5). The maximum luminance achieved is ~23 000 cd/m^2 (NPB-Si$_2$), ~36 000 cd/m^2 (TPD-Si$_2$), and ~14 000 cd/m^2 (NPB-only). Maximum forward external quantum efficiencies are 0.8% (NPB-Si$_2$), 1.6% (TPD-Si$_2$), and 1.87% (NPB-only). The operating bias for 300 cd/m^2 is 7.0, 7.0, and 10.5 V for NPB-Si$_2$, TPD-Si$_2$, and NPB-only, respectively. In Table 3, the EL response data are compared among devices using NPB-Si$_2$ and TPD-Si$_2$ SAMs, spin-cast NPB-Si$_2$ and TPD-Si$_2$ films, and NPB-only as the HTL, respectively. OLEDs with spin-cast TPD-Si$_2$ films as the HTL exhibit more than a 2-fold increase of maximum luminance, ~50% lower turn-on voltage, and comparable external forward quantum efficiency versus those of devices having NPB only as the HTL.
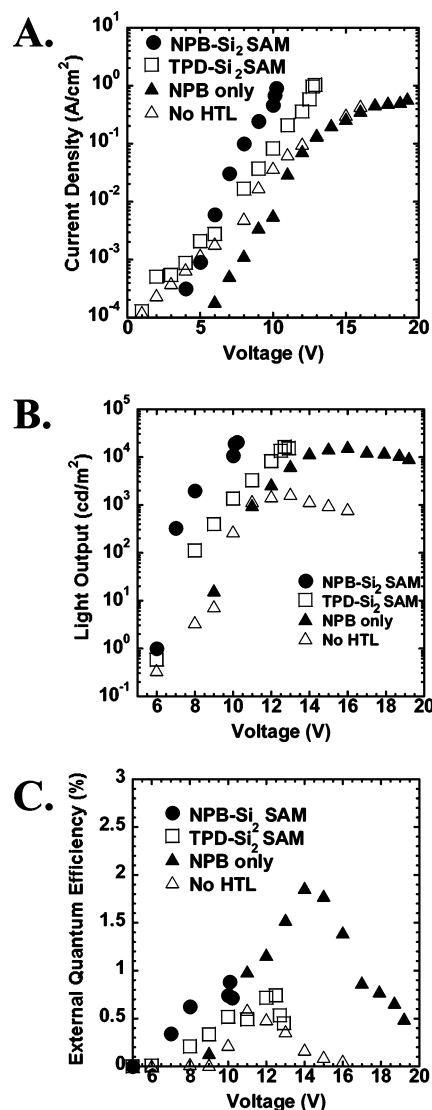
(62) Napper, A. M.; Liu, H. Y.; Waldeck, D. H. *J. Phys. Chem. B* **2001**, *105*, 7699−7707.
(63) Nahir, T. M.; Clark, R. A.; Bowden, E. F. *Anal. Chem.* **1994**, *66*, 2595−2598.
(64) Forster, R. J. *Inorg. Chem.* **1996**, *35*, 3394−3403.

Figure 4. Responses of OLEDs having structures ITO/HTL/Alq: 1% DIQA (60 nm)/BCP:Li (20 nm)/Al (100 nm), HTL = NPB-Si$_2$ SAM (1.4 nm), TPD-Si$_2$ SAM (1.7 nm), NPB (20 nm) only. (A) Current density versus voltage; (B) luminance versus voltage; (C) external forward quantum efficiency versus voltage.

Applying TPD-Si$_2$ and NPB-Si$_2$ SAMs as ITO Anode−NPB Interlayers. OLED EL Response. Self-assembled TPD-Si$_2$ and NPB-Si$_2$ films can also be applied as interlayers between the ITO anode and the conventional NPB HTL in OLEDs having structures ITO anode/SAM/NPB/Alq doped with DIQA/BCP/Li/Al. Insertion of these interlayers between the anode and the NPB HTL dramatically enhances OLED EL response as compared to devices without the interlayers (Figure 6). As compared to OLEDs using TPD-Si$_2$ or NPB-Si$_2$ SAMs as the HTLs, which are directly in contact with the EML (Figure 4), the maximum light output is enhanced by a factor of ~3× both for TPD-Si$_2$- and for NPB-Si$_2$-based devices: ~18 000 cd/m^2 → 50 000 cd/m^2 (NPB-Si$_2$/NPB), ~17 000 cd/m^2 → 45 000 cd/m^2 (TPD-Si$_2$/NPB). Likewise, the maximum forward external quantum efficiency is increased to 1.8% (NPB-Si$_2$/NPB) and 2.3% (TPD-Si$_2$/NPB) versus 0.8% (NPB-Si$_2$), 0.75% (TPD-Si$_2$), and 1.87% (NPB alone).

(65) Richardson, J. N.; Rowe, G. K.; Carter, M. T.; Tender, L. M.; Curtin, L. S.; Peck, S. R.; Murray, R. W. *Electrochim. Acta* **1995**, *40*, 1331−1338.
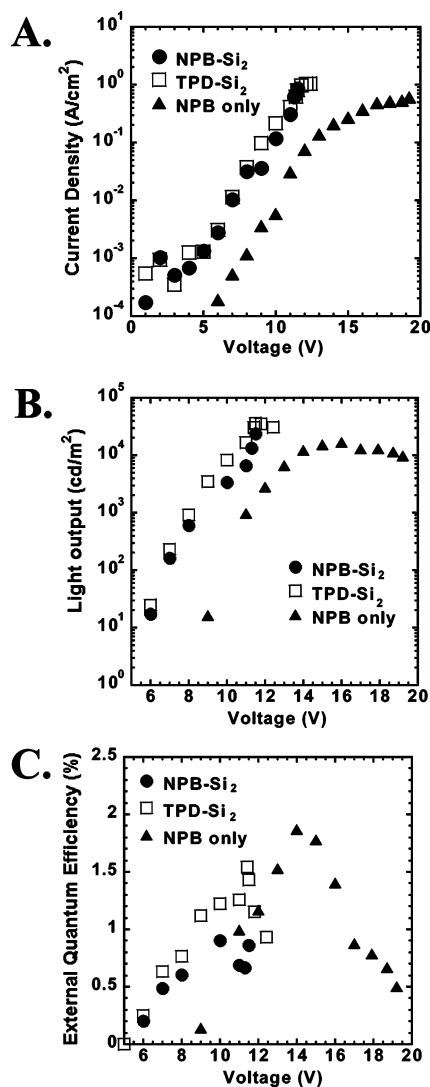
Figure 5. Responses of OLEDs having structures ITO/HTL/Alq: 1% DIQA (60 nm)/BCP:Li (20 nm)/Al (100 nm), HTL = spin-cast NPB-Si$_2$ film (40 nm), spin-cast TPD-Si$_2$ film (40 nm), and NPB (20 nm) only. (A) Current density versus voltage; (B) luminance versus voltage; (C) external forward quantum efficiency versus voltage.

Spin-Cast TPD-Si$_2$ and NPB-Si$_2$ Films as ITO Anode–NPB Interlayers. OLED EL Response. Spin-casting TPD-Si$_2$ or NPB-Si$_2$ layers onto ITO anodes, followed by vapor-deposition of NPB, was also investigated as an alternative approach to applying these silanes as the anode–NPB interlayers. Again, improved EL response is observed versus that of OLEDs without interlayers and versus devices fabricated with only spin-coated films as HTLs (Figure 7): maximum light output, ~46 000 cd/m^2 (NPB-Si$_2$/NPB), ~64 000 cd/m^2 (TPD-Si$_2$/NPB) versus ~23 000 cd/m^2 (NPB-Si$_2$), ~36 000 cd/m^2 (TPD-Si$_2$), ~14 000 cd/m^2 (NPB-only); maximum forward external quantum efficiencies, 2.4% (NPB-Si$_2$/NPB), 2.3% (TPD-Si$_2$/NPB) versus 0.8% (NPB-Si$_2$), 1.6% (TPD-Si$_2$), 1.87% (NPB-only); turn-on voltages, 4.0 V (NPB-Si$_2$/NPB), 6 V (TPD-Si$_2$/NPB) versus 5.0 V (NPB-Si$_2$), 5.0 V (TPD-Si$_2$), 9.0 V (NPB-only). In Table 4, the EL response data are compared for devices using NPB-Si$_2$ and TPD-Si$_2$ SAMs, as well as spin-cast NPB-Si$_2$ and TPD-Si$_2$ films as ITO anode–NPB interlayers, respectively.

Hole-Only Devices. Hole-only devices were fabricated to investigate the effect of NPB-Si$_2$ and TPD-Si$_2$ SAM coatings
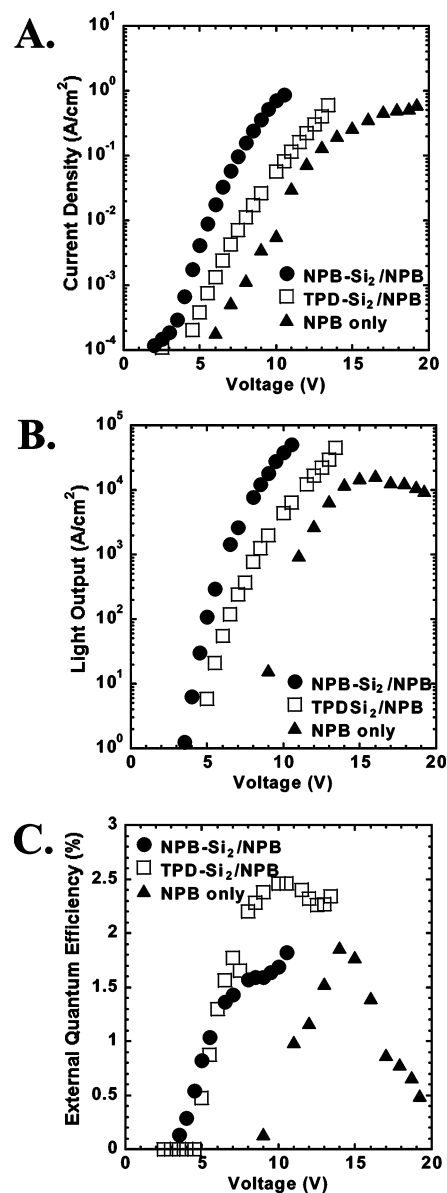

Figure 6. Responses of OLEDs having structures ITO/HTL SAM/NPB (20 nm)/Alq: 1% DIQA (60 nm)/BCP:Li (20 nm)/Al (100 nm), HTL SAM = NPB-Si$_2$ SAM and TPD-Si$_2$ SAM. (A) Current density versus voltage; (B) luminance versus voltage; (C) external forward quantum efficiency versus voltage.

on hole injection efficiency from the ITO anode into the NPB HTL.[65] I–V characteristics were measured on devices having structure ITO/siloxane/NPB(400 nm)/Au (6 nm)/Al (Figure 8). Orders of magnitude larger hole currents are observed for devices with the siloxane SAMs as ITO anode–NPB interlayers, indicating strong hole injection enhancement by modifying the anode with NPB-Si$_2$ and TPD-Si$_2$, respectively. Attempting to measure hole fluence through either the self-assembled or the spin-coated siloxane films in ITO/siloxane/Au/Al structures yielded irreproducible results, presumably due to the leakage currents in such device configurations.

3.3. Saturated Alkyl Siloxane SAMs as OLED Anode Functionalization Layers. Saturated Alkyl Siloxane SAM HTLs in OLEDs. To further understand the function of TPD-Si$_2$, NPB-Si$_2$, and similar interlayers in OLEDs, saturated alkylsilanes having varied alkyl chain length (Scheme 2) were

Table 3. OLED EL Response Data for Devices Having the Structure ITO Anode/HTL/Alq Doped with DIQA/BCP Doped with Li/Al[a]

	no HTL	NPB-Si$_2$ SAM	TPD-Si$_2$ SAM	NPB-Si$_2$ (spin-coated)	TPD-Si$_2$ (spin-coated)	NPB-only
maximum luminance (cd/m^2)	~1500	~18 000	~17 000	~23 000	~36 000	~14 000
maximum external forward quantum efficiency (%)	0.6	0.8	0.75	0.8	1.6	1.87
turn-on voltage (V)	9.0	4.6	5.5	5.0	5.0	9.0
operating voltage at 300 cd/m^2 (V)	10.5	8.0	8.5	7.0	7.0	10.5

[a] The HTL is NPB-Si$_2$ SAMs, TPD-Si$_2$ SAMs, spin-cast NPB-Si$_2$ films, spin-cast TPD-Si$_2$ films, and vapor deposited NPB alone, respectively.
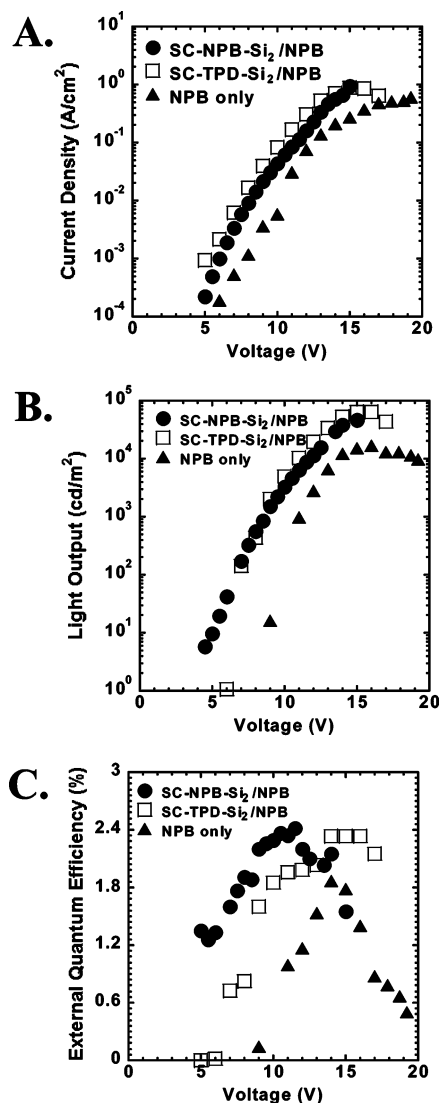

Figure 7. Responses of OLEDs having structures ITO/spin-cast HTL/NPB (20 nm)/Alq:1% DIQA (60 nm)/BCP:Li (20 nm)/Al (100 nm), spin-cast HTL = spin-cast NPB-Si$_2$ film and TPD-Si$_2$ film. (A) Current density versus voltage; (B) luminance versus voltage; (C) external forward quantum efficiency versus voltage.
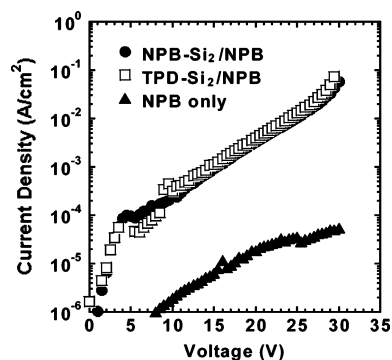

Figure 8. Evaluation of hole injection properties of anode SAM functionalization layers NPB-Si$_2$ and TPD-Si, comparing I−V response for hole-only devices having the structure ITO/HTL SAM/NPB(400 nm)/Au(6 nm)/Al (120 nm).

self-assembled onto ITO surfaces, forming nanometer-thick SAMs. In contrast and not unexpectedly, smooth and uniform films could not be fabricated by spin-casting due to inefficient cross-linking: the silanes have only a single trichlorosilyl group per molecule. These silanes do not have hole transporting triarylamine motifs as TPD-Si$_2$ and NPB-Si$_2$, but covalently modify the ITO anode via silane condensation in a phenomenologically manner similar to TPD-Si$_2$ and NPB-Si$_2$. I−V−L characteristics of OLEDs having the structure ITO anode/alkylsiloxane SAM/Alq doped with DIQA/BCP/Li/Al were compared to

TPD-Si$_2$ SAM-based OLEDs as well as to devices having no HTL (Figure 9, NPB-Si$_2$ SAM data omitted for clarity; refer to Figure 4 for comparison between TPD-Si$_2$ and NPB-Si$_2$ SAMs). Note that the ITO/*n*-butylsiloxane SAM/Alq OLED exhibits efficiency and luminance greater than those of the TPD-Si$_2$ SAM-based devices, with a maximum luminance of ~26 000 cd/m^2 and a maximum forward external quantum efficiency ~1.5% at 15 V. Also, the device performance is competitive with that of NPB-based OLEDs. Interestingly, pronounced alkyl chain length effects on the EL response are observed. For instance, the maximum light output is 5000 cd/m^2 (methyl), 26 000 cd/m^2 (*n*-butyl), 13 000 cd/m^2 (*n*-octyl), and 60 cd/m^2 (*n*-octadecyl), and forward external quantum efficiency is 0.4% (methyl), 1.5% (*n*-butyl), 1.1% (*n*-octyl), and 0.025% (*n*-octadecyl). In Table 5, the EL response is compared among devices using alkylsiloxane SAMs, a TPD-Si$_2$ SAM, and NPB alone as HTLs.

Saturated Alkyl Siloxane SAMs as ITO Anode−NPB Interlayers. OLED EL Response. Similar to the experiments with TPD-Si$_2$ and NPB-Si$_2$ SAMs, alkyl siloxane SAMs were self-assembled onto ITO anodes, followed by vapor deposition of 20 nm thick NPB, so that the SAMs function as anode−NPB interlayers in OLEDs having structures ITO anode/SAM/NPB/Alq doped with DIQA/BCP/Li/Al. I−V−L characteristics were measured and are shown in Figure 10. As compared to OLEDs without anode−HTL interlayers, orders of magnitude increased (methyl, *n*-butyl, and *n*-octyl siloxane SAMs) or decreased (*n*-octadecyl siloxane SAM) levels of current density, light output, and quantum efficiency at identical bias are observed, indicating dramatic effects on hole injection efficiency are effected by depositing the nanometer-thick alkylsiloxane layers on the ITO anode surface. For example, at 10 V, the light output is 7500 cd/m^2 (methyl SAM/NPB), 6500 cd/m^2 (*n*-butyl SAM/NPB), 7100 cd/m^2 (*n*-octyl SAM/NPB), <1 cd/m^2 (*n*-octadecyl SAM/NPB), and 110 cd/m^2 (NPB-only). Furthermore, the forward external quantum efficiency is 1.8% (methyl

Table 4. OLED EL Response Data for Devices Having the Structure ITO Anode/Interlayer/NPB/Alq Doped with DIQA/BCP Doped with Li/Al[a]

	NPB-Si$_2$ SAM	TPD-Si$_2$ SAM	NPB-Si$_2$ (spin-coated)	TPD-Si$_2$ (spin-coated)	NPB-only
maximum luminance (cd/m^2)	~50 000	~45 000	~46 000	~64 000	~14 000
maximum external forward quantum efficiency (%)	1.8	2.3	2.4	2.3	1.87
turn-on voltage (V)	3.5	5.0	4.0	6.0	9.0
operating voltage at 300 cd/m^2 (V)	5.5	7.2	7.2	7.0	10.5

[a] The interlayer is an NPB-Si$_2$ SAM, a TPD-Si$_2$ SAM, a spin-cast NPB-Si$_2$ film, or a spin-cast TPD-Si$_2$ film.
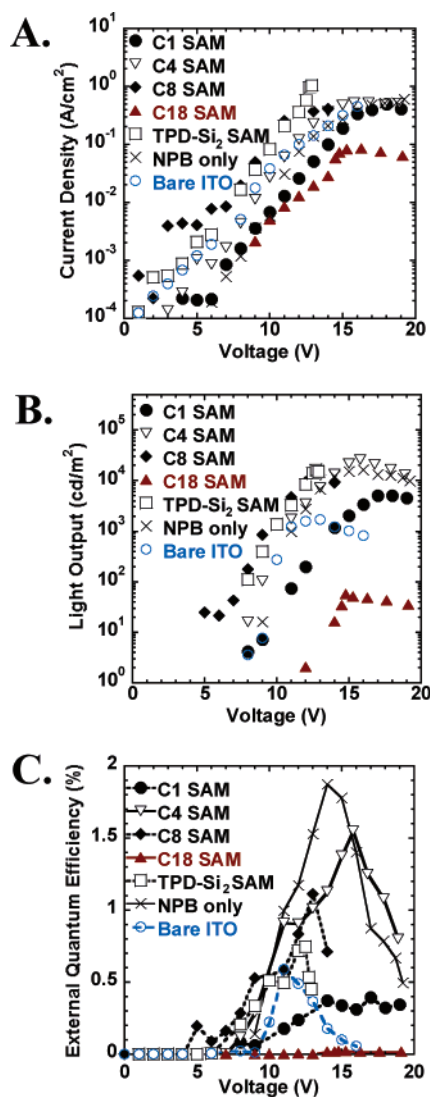

Figure 9. Responses of OLEDs having structures ITO/HTL SAM/Alq: 1% DIQA (60 nm)/BCP:Li (20 nm)/Al (100 nm); HTL = methylsiloxane SAM (C1), n-butylsiloxane SAM (C4), n-octylsiloxane SAM (C8), n-octadecylsiloxane SAM (C18), TPD-Si$_2$, and NPB. (A) Current density versus voltage; (B) luminance versus voltage; (C) external forward quantum efficiency versus voltage. Lines through the data points are drawn as a guide to the eye.

SAM/NPB), 1.5% (n-butyl SAM/NPB), 1.5% (n-octyl SAM/NPB), 0.24% (n-octadecyl SAM/NPB), and 0.5% (NPB-only). Similar to using a TPD-Si$_2$ SAM as the anode−NPB interlayer, the alkylsiloxane SAMs with short alkyl chains result in significant OLED performance enhancement as ITO anode−NPB interlayers. In Table 6, EL response is compared among devices using the alkylsiloxane SAMs and a TPD-Si$_2$ SAM as ITO anode−NPB interlayers.

4. Discussion

Replacing Conventional HTLs with TPD-Si$_2$- and NPB-Si$_2$-Based Materials. Relationships between ITO Anode−HTL Contact and OLED Hole Injection Efficiency and EL Response (Turn-on Voltage, Luminance). It has been demonstrated here that TPD-Si$_2$ and NPB-Si$_2$, with hole transporting structural motifs similar to those of traditional triarylamine HTLs such as TPD and NPB, respectively, can be self-assembled or spin-cast onto the ITO anode surface, utilizing the reactive trichlorosilyl functionalities to covalently graft the structure to the surface. OLEDs having TPD-Si$_2$- and NPB-Si$_2$-based materials as the HTLs exhibit good EL response (Figures 4 and 5, Table 3). As new HTL materials, TPD-Si$_2$ and NPB-Si$_2$ fulfill the generally accepted requirements for efficacious HTLs: (1) they possess electronic levels energetically comparable to those of TPD and NPB according to UPS measurements (Scheme 5); (2) they form smooth, conformal, uniform, and electroactive films on ITO surfaces; (3) the films are strongly adherent and thermally stable,[67] and (4) the degree of physical contact achieved between these HTLs and the ITO surface is not available to conventional HTLs. To date, in all reported polymeric and in many reported small molecule OLEDs, HTLs such as TPD, NPB, and poly(3,4-ethylenedioxythiophene)-poly(styrenesulfonate) (PEDOT-PSS) (Scheme 1) are deposited directly onto the ITO anode by either thermal evaporation or spin-coating, resulting in anode−HTL contact that is largely physical in character. This interface is prone to large contact resistance, which is detrimental to OLED EL response.[68] Furthermore, thermally induced delamination/dewetting is also observed at ITO anode−TPD or NPB interfaces due to severe surface energy mismatches, [69−71] and in some cases, traditional HTL materials cause extensive ITO corrosion.[72,73] Thermally induced interfacial morphology changes are also observed on copper phthalocyanine buffer layers.[69,74] In contrast, TPD-Si$_2$ and NPB-Si$_2$ form covalent bonds to the ITO surface, ensuring strong adhesion and, via close surface energy matching, intimate ITO anode−HTL physical and electrical contact.[47] The improved light output and hole injection efficiency, and reduced turn-on voltages versus conventional ITO/NPB interfaces (Figures 4, 5, and 8), demonstrate that such contact is crucial to good device performance and should be considered in designing new HTL materials. Interestingly, the magnitudes of hole current across

(66) Crone, B. K.; Campbell, I. H.; Davids, P. S.; Smith, D. L. *Appl. Phys. Lett.* **1998**, *73*, 3162−3164.

(67) Huang, Q. L.; Cui, J.; Marks, T. J. *Abstr. Pap. Am. Chem. Soc.* **2002**, *224*, POLY 032−033.

(68) Shen, Y.; Klein, M. W.; Jacobs, D. B.; Scott, J. C.; Malliaras, G. G. *Phys. Rev. Lett.* **2001**, *86*, 3867−3869.

(69) Cui, J.; Huang, Q.; Veinot, J. C. G.; Yan, H.; Wang, Q.; Hutchison, G. R.; Richter, A. G.; Evmenenko, G.; Dutta, P.; Marks, T. J. *Langmuir* **2002**, *18*, 9958−9970.

(70) Cui, J.; Huang, Q.; Veinot, J. G. C.; Yan, H.; Marks, T. J. *Adv. Mater.* **2002**, *14*, 565−567.

Table 5. Comparative OLED EL Response Data for Devices Having the Structure ITO Anode/HTL/Alq Doped with DIQA/BCP Doped with Li/Al[a]

HTL	methylsiloxane SAM	*n*-butylsiloxane SAM	*n*-octylsiloxane SAM	*n*-octadecylsiloxane SAM	TPD-Si$_2$ SAM	NPB-only
maximum luminance (cd/m^2)	~5000	~26 000	~13 000	~60	~17 000	~14 000
maximum external forward quantum efficiency (%)	0.4	1.5	1.1	0.025	0.75	1.87
turn-on voltage (V)	7.5	7.5	6	12	5.5	9
operating voltage at 300 cd/m^2 (V)	12.5	9.5	9.5		8.5	10.5

[a] HTL = a methylsiloxane SAM, an *n*-butylsiloxane SAM, an *n*-octylsiloxane SAM, an *n*-octadecylsiloxane SAM, a TPD-Si$_2$ SAM, and vapor-deposited NPB alone.
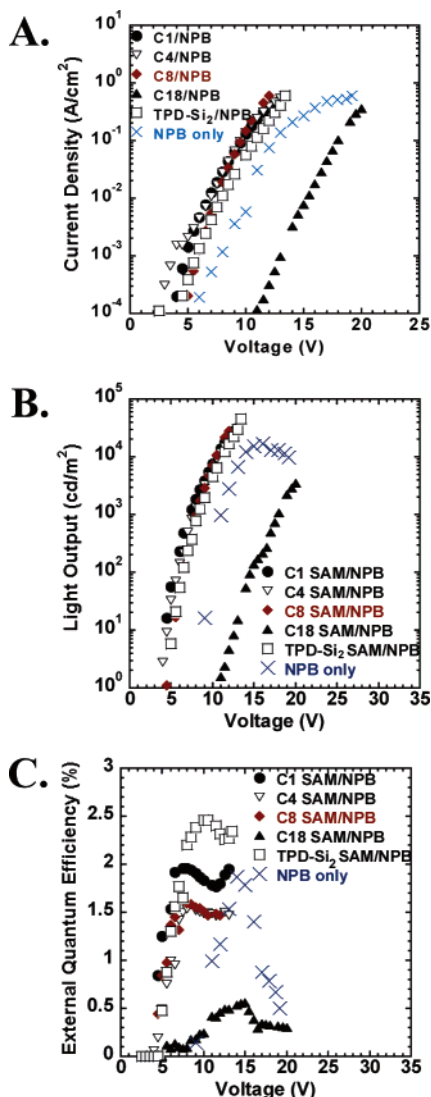

Figure 10. Responses of OLEDs having the structures ITO/HTL SAM/NPB (20 nm)/Alq: 1% DIQA (60 nm)//BCP:Li (20 nm)/Al (100 nm), HTL SAM = methylsiloxane SAM (C1), *n*-butylsiloxane SAM (C4), *n*-octylsiloxane SAM (C8), *n*-octadecylsiloxane SAM (C18), and TPD-Si$_2$. (A) Current density versus voltage; (B) luminance versus voltage; (C) external forward quantum efficiency versus voltage.

the ITO anode−TPD-Si$_2$ or NPB-Si$_2$ SAM interfaces are very similar, indicating that the contact rather than the details of hole transporting motif must play a significant role. However, the ITO/siloxane SAM OLEDs have somewhat lower forward external quantum efficiencies than conventional ITO/NPB devices (Figure 4 and Table 3), which is explained below.

Replacing Conventional HTLs with TPD-Si$_2$- and NPB-Si$_2$-Based Materials. Effects on External Forward Quantum

Scheme 5. Energy Diagram for the Electrodes and Organic Layers Employed in This Study (Taken from Literature Data)
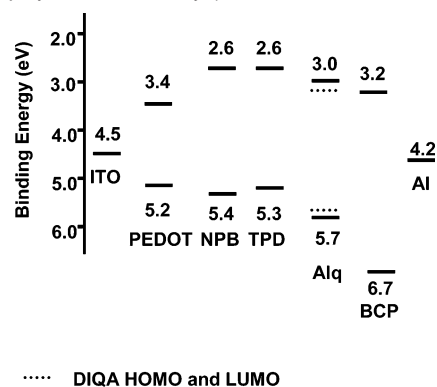
Efficiency. Note that replacing a conventional HTL (NPB) with very thin siloxane SAMs results in devices with significantly diminished external forward quantum efficiency. This is attributed to a possible efficiency loss mechanism: as compared to ~20 nm thick NPB HTL, TPD-Si$_2$ and NPB-Si$_2$ SAMs are likely to have reduced electron-blocking properties due to their nanometer scale thickness. It has been recently argued that a minimum of ~20 nm NPB is required to effectively block electrons from unproductively leaking to the ITO anode.[75] Possibly the ~1.5 nm thick TPD-Si$_2$ and NPB-Si$_2$ SAMs are not sufficiently thick to prevent all electrons from escaping the emissive HTL/EML (Alq) interfacial zone. This hypothesis is supported by the device efficiency recovery in the case of ~40 nm thick spin-coated TPD-Si$_2$ as the HTL, due to increased HTL thickness and, within this explanation, more efficient electron-blocking properties that outweigh thickness effects. Also, the dramatic efficiency increase in OLEDs having the SAMs as ITO anode−HTL interlayers versus as the only HTLs (Figure 6 vs Figure 4) can be explained on the basis of the superior electron-blocking properties of the combined NPB + SAM layer. Here, the enhanced ITO-NPB physical/electrical contact provided by the SAM is combined with the far more favorable electron-blocking characteristics. However, the above explanation does not completely explain the modest external forward quantum efficiency gain when ~1.5 nm NPB-Si$_2$ SAM is replaced with a ~40 nm spin-coated NPB-Si$_2$ film (Figures 4, 5 and Table 3). We speculate there are other factors influencing the efficiency here. One reasonable explanation is

(71) Cui, J.; Wang, Q.; Marks, T. J. *Polym. Mater. Sci. Eng.* **2000**, *83*, 239−240.
(72) de Jong, M. P.; de Voigt, M. J. A. *Appl. Phys. Lett.* **2000**, *77*, 2255−2257.
(73) Ni, J.; Wang, A.; Yang, Y.; Stern, C. L.; Metz, A. W.; Jin, S.; Wang, L.; Marks, T. J.; Kannewurf, C. R. *J. Am. Chem. Soc.* **2005**, *127*, 5613−5624.
(74) Xu, M. S.; Xu, J. B. *J. Phys. D: Appl. Phys.* **2004**, *37*, 1603−1608.
(75) Zhang, S. T.; Wang, Z. J.; Zhao, J. M.; Zhan, Y. Q.; Wu, Y.; Zhou, Y. C.; Ding, X. M.; Hou, X. Y. *Appl. Phys. Lett.* **2004**, *84*, 2916−2918.

Table 6. Comparative OLED EL Response Data for Devices Having the Structure ITO Anode/Interlayer/NPB/Alq Doped with DIQA/BCP Doped with Li/Al[a]

interlayer	methylsiloxane SAM	*n*-butylsiloxane SAM	*n*-octylsiloxane SAM	*n*-octadecylsiloxane SAM	TPD-Si$_2$ SAM	NPB-only
maximum luminance (cd/m^2)	~30 000	~25 000	~28 000	~3500	~45 000	~14 000
maximum external forward quantum efficiency (%)	1.8	1.5	1.5	0.5	2.3	1.87
turn-on voltage (V)	4.2	4.0	4.5	11	5.0	9
operating voltage at 300 cd/m^2 (V)	6.2	6.7	7.0	16.8	7.2	10.5

[a] The interlayer is a methylsiloxane SAM, an *n*-butylsiloxane SAM, an *n*-octylsiloxane SAM, an *n*-octadecylsiloxane SAM, and a TPD-Si$_2$ SAM.

concerned with the mechanism of siloxane film formation on hydroxylated surfaces,[49,76] in which incomplete thermal cross-linking may result in residual, uncondensed silanol functionalities.[77] Such Si−OH groups are known to induce the chemical degradation of Alq[78,79] and are likely to react with mobile electrons and holes. Furthermore, it has been reported that radical ions generated under high electric fields in operating OLEDs can quench fluorescent dye dopant emission via direct resonant energy transfer from excited states to quenching centers.[80] It is conceivable that Si−OH functionalities act as quenchers.[81] The energy transfer rate is related to the excited state-quenching center distance by eq 3, where *r* is the energy transfer rate, *d* is the separation between excited states and quenching centers, and *x* depends on the nature of the interaction between excited states and quenching centers.[80]

$$r \propto d^{-x} \qquad (3)$$

When siloxanes are used as HTLs, the EML (Alq) is deposited directly on top of siloxane films, forming a HTL/EML interface where hydroxyl groups may be present. Because the Alq electron mobility is orders of magnitude greater than the hole mobility, holes and electrons should primarily recombine at or near HTL/EML interface, forming emissive excitons.[82] Some of these may be quenched/decomposed by hydroxyl groups in this region, via the aforementioned mechanisms. The observation that thicker spin-coated NPB-Si$_2$ HTL does not significantly improve external forward quantum efficiency (Table 3) may be attributable to the presence of uncondensed hydroxyl functionalities functioning as impurities/quenching centers.[78,83] The quenching effect appears to work against the increased electron-blocking properties of the thicker NPB-Si$_2$ films and results in the overall similar external forward quantum efficiencies for SAM and spin-coated NPB-Si$_2$ HTL-based OLEDs. TPD-Si$_2$ may undergo more complete cross-linking as indicated by the more distorted cyclic voltammetric curve shape than that of NPB-Si$_2$ (Figure 3) and the weaker intensity of the silanol OH vibration transitions at 3150−3700 cm^{-1} in FTIR spectra (Figure 11), suggesting more complete siloxane formation and correspondingly diminished reactivity and emissive
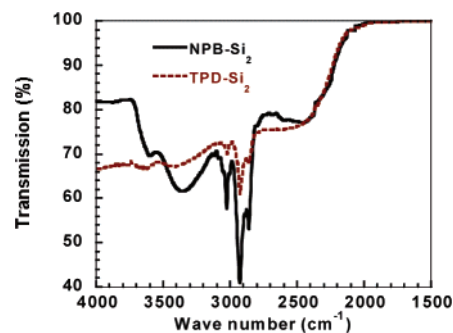

Figure 11. FTIR spectra of 40 nm TPD-Si$_2$ and NPB-Si$_2$ films spin-cast and cured on glass substrates under the same conditions (bare glass substrate absorption baseline subtracted).

state quenching. In this case, the effects of increased electron-blocking with greater TPD-Si$_2$ film thickness are dominant, affording enhanced external forward quantum efficiency via replacing a TPD-Si$_2$ SAM HTL with a spin-coated one (Table 3). In this scenario, the excitons must be spatially removed from the silanol functionalities to minimize reaction and quenching, which can be realized by using the siloxanes as ITO anode−NPB interlayers, as discussed below.

Self-Assembled and Spin-Coated TPD-Si$_2$ and NPB-Si$_2$ Materials as ITO Anode−NPB Interlayers. As shown in Figures 6, 7 and Table 4, significantly greater EL response, including forward external quantum efficiency, is achieved by using the TPD-Si$_2$ or NPB-Si$_2$ materials as the anode−NPB interlayers versus applying them as the only HTL. This supports the above discussion because (1) a ~20 nm thick NPB layer deposited on the interlayers enhances the electron-blocking properties; (2) the NPB/Alq interface replaces the TPD-Si$_2$/Alq or NPB-Si$_2$/Alq interface when the siloxanes are used as the ITO anode−NPB interlayer, and thus the exciton recombination region is at or very near the NPB/Alq interface, tens of nanometers away from the siloxane structure. Any reactivity or exciton quenching by silanol functionalities should be greatly reduced according to eq 3.

In addition, the substantial OLED EL response enhancement obtained by inserting the various siloxane structures between the ITO anode and the NPB HTL, as compared to ITO/NPB, can be plausibly explained on the basis of the current understanding of ITO anode−HTL interfacial function. To date, a variety of explanations for the effects of ITO anode−HTL interlayers have been proposed, including increased hole injection via dipole moment-induced additional electric fields,[30] reduced injected charge backscattering,[32] decreased anode work function-HTL HOMO energetic barriers,[84] increased recombination efficiency via balancing electron and hole injection,[31,85] and/

(76) Silberzan, P.; Leger, L.; Ausserre, D.; Benattar, J. J. *Langmuir* **1991**, *7*, 1647−1651.
(77) Zhao, X.; Kopelman, R. *J. Phys. Chem.* **1996**, *100*, 11014−11018.
(78) Liao, L. S.; He, J.; Zhou, X.; Lu, M.; Xiong, Z. H.; Deng, Z. B.; Hou, X. Y.; Lee, S. T. *J. Appl. Phys.* **2000**, *88*, 2386−2390.
(79) Xu, M. S.; Xu, J. B.; Chen, H. Z.; Wang, M. *J. Phys. D: Appl. Phys.* **2004**, *37*, 2618−2622.
(80) Young, R. H.; Tang, C. W.; Marchetti, A. P. *Appl. Phys. Lett.* **2002**, *80*, 874−876.
(81) Schaer, M.; Nesche, F.; Berner, D.; Leo, W.; Zuppiroli, L. *Adv. Funct. Mater.* **2001**, *11*, 116−120.
(82) Kondakov, D. Y.; Sandifer, J. R.; Tang, C. W.; Young, R. H. *J. Appl. Phys.* **2003**, *93*, 1108−1119.
(83) Aziz, H.; Popovic, Z.; Tripp, C. P.; Hu, N.; Hor, A.; Xu, G. *Appl. Phys. Lett.* **1998**, *72*, 2642−2644.

(84) Lee, S. T.; Wang, Y. M.; Hou, X. Y.; Tang, C. W. *Appl. Phys. Lett.* **1998**, *74*, 670−672.

or confining electrons to the emissive layer.[33] Surface energy-promoted wetting/cohesion at the ITO−organic layer interface is also known to be a significant factor.[1,43,70,74] According to these arguments, we propose that the TPD-Si$_2$ and NPB-Si$_2$ materials, when employed as ITO anode−NPB interlayers, increase hole injection principally by: (1) reducing the hole injection barrier from the ITO anode to NPB (HOMO ∼ 5.5 eV) by providing an energy-mediating step (Table 2); (2) enhancing ITO anode−NPB interfacial cohesion via eliminating the surface energy mismatch;[69] and (3) contributing to the aforementioned electron confinement effects in conjunction with NPB. Any interfacial dipole effects would appear to be relatively small as indicated by the small UPS-determined ±0.1 eV vacuum level shift (Table 2), and cannot be fully responsible for the dramatic EL response enhancement evident in Figures 6, 7 and in Table 4. The effect of TPD-Si$_2$ and NPB-Si$_2$ interlayers on balancing electron and hole injection will be discussed below. Overall, these factors contribute to improved hole injection and device performance.

Alkylsiloxane SAMs as HTLs in OLEDs. In a conventional picture, OLED response should be eroded in the absence of a triarylamine functionality interposed between the anode and the EML/ETL. Interestingly, however, we find that replacing NPB with *n*-butylsiloxane SAMs (Scheme 2) results in appreciable increase in EL response (maximum light output = 26 000 cd/m^2 (*n*-butyl) vs 16 000 cd/m^2 (NPB-only); forward external quantum efficiency 1.5% (*n*-butyl) vs 1.9% (NPB-only), Figure 9). In contrast, replacing NPB with methylsiloxane or *n*-octadecylsiloxane leads to significantly diminished EL response (Figure 9, Table 5). The poor EL response of OLEDs having the *n*-octadecylsiloxane SAM can be readily explained from established relationships between distance-dependent charge carrier tunneling efficiency and alkylsiloxane SAM chain length.[86−88] Here, tunneling is believed to be the primary charge transport mechanism through alkylsiloxane SAMs and follows eq 4:[88,89]

$$i = i_0 \exp(-\beta d) \qquad (4)$$

where *d* is the thickness of barrier through which the electron tunneling takes place, and *β* is the tunneling coefficient (0.64−1.16^{-1} for alkanethiol monolayers on gold[90]). The thickness of the methylsiloxane, *n*-butylsilxoane, *n*-octyl-, and *n*-octadecyl-siloxane SAMs is reported to be 2.8, 6.2, 8.0, and 23 Å,[91] respectively. In the case of the SAMs with short alkyl chains, it is reasonable that significant hole injection from the ITO anode into the EML can occur via tunneling through the very thin SAMs, while in the case of the *n*-octadecylsiloxane SAM, the tunneling becomes inefficient and the insulating properties dominate.[88,92,93] This can explain the dramatically decreased current density, light output, and forward external quantum efficiency seen in Figure 9, due to the significant energy barrier
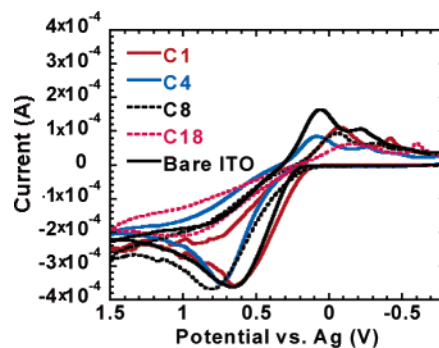

Figure 12. Comparative cyclic voltammetry characteristics of self-assembled alkylsiloxane-coated ITO electrodes in ferrocene solution. The SAMs are methylsiloxane SAM (C1), *n*-butylsiloxane SAM (C4), *n*-octylsiloxane SAM (C8), and *n*-octadecylsiloxane SAM (C18). SAM-coated ITO, silver wire, and Pt wire were used as the working electrode, reference electrode, and counter electrode, respectively. All experiments were carried out in 0.1 M acetonitrile solution of tetrabutylammonium hexafluorophosphate as the electrolyte and 0.001 M ferrocene as the internal pinhole probe at scan rate 0.1 V/s.

for effective hole tunneling from the ITO anode through the *n*-octadecylsiloxane SAM into the Alq emissive layer.

Further discussion is appropriate to explain the lower forward external quantum efficiencies of OLEDs using the very thin methylsiloxane SAM as the HTL versus *n*-butyl- and *n*-octyl-siloxane SAMs (Figure 9), even though all of the SAMs should support efficient charge carrier tunneling according to the above arguments. We suggest that methylsiloxane SAM has poorer electron-blocking properties than *n*-butyl- and *n*-octylsiloxane SAMs due to, among other factors, greater defect densities. It is reported that SAM defects are correlated with the alkyl chain length, with longer chains leading to SAMs with less defects.[94] In ITO/SAM/Alq OLEDs, the SAM defects may provide pathways for electrons to escape the SAM/Alq interfacial region, and reduce the SAM electron-blocking function, which is a critical requirement for high-performance HTLs.[75] Greater defect densities for the methylsiloxane SAM than for the *n*-butyl- or *n*-octylsiloxane SAM would result in less efficient electron-blocking and hole-electron recombination, consequently lowering device efficiency.

To probe the presence of SAM defects, cyclic voltammetry experiments using ferrocene as a redox probe were carried out using the above SAM-coated ITO substrates as working electrodes (Figure 12). The results of these experiments are consistent with the above hypothesis. In the case of the methylsiloxane SAM, ferrocene redox peaks are observed, which are largely unchanged from those observed with bare ITO, suggesting significant defect densities are present in the SAM layer, which provide uninhibited ferrocene oxidation at the ITO electrode surface. In the cases of *n*-butyl and *n*-octyl siloxane SAMs, the apparent defect densities vary significantly with film deposition conditions. Presumably, trace amounts of water have large effects on SAM quality.[49] SAMs with lower pinhole densities, indicated by the shifted ferrocene oxidation peak potential, lead to higher OLED efficiency seen in Figure 9. Finally, the *n*-octadecylsiloxane SAM extensively passivates the ITO surface, as judged both by the large separation between

(85) Forsythe, E. W.; Abkowitz, M. A.; Gao, Y. *J. Phys. Chem. B* **2000**, *104*, 3948−3952.
(86) Chidsey, C. E. D.; Bertozzi, C. R.; Putvinski, T. M.; Mujsce, A. M. *J. Am. Chem. Soc.* **1990**, *112*, 4301−4306.
(87) Smalley, J. F.; Feldberg, S. W.; Chidsey, C. E. D.; Linford, M. R.; Newton, M. D.; Liu, Y. P. *J. Phys. Chem.* **1995**, *99*, 13141−13149.
(88) Chidsey, C. E. *Science* **1991**, *251*, 919−922.
(89) Parker, I. D. *J. Appl. Phys.* **1994**, *75*, 1656−1666.
(90) Zhao, J.; Uosaki, K. *J. Phys. Chem. B* **2004**, *108*, 17129−17135 and references therein.
(91) Jin, Z. H.; Vezenov, D. V.; Lee, Y. W.; Zull, J. E.; Sukenik, C. N.; Savinell, R. F. *Langmuir* **1994**, *10*, 2662−2671.

(92) Wang, B.; Luo, J.; Wang, X.; Wang, H.; Hou, J. G. *Langmuir* **2004**, *20*, 5007−5012.
(93) Lercel, M. J.; Whelan, C. s.; Craighead, H. G.; Seshadri, K.; Allara, D. L. *J. Vac. Sci. Technol., B* **1996**, *14*, 4085−4090.
(94) Ohtake, T.; Mino, N.; Kazufumi, O. *Langmuir* **1992**, *8*, 2081−2083.

ferrocene anodic and cathodic peaks and by the overall magnitude of current flowing at any potential.[95] Note that the aqueous advancing contact angles for the above SAMs on ITO glass substrates are all similar ($90 \pm 5°$), making the correlation between SAM defects and contact angle indexed surface energies inconclusive.[76]

The SAM alkyl chain length effects on OLED response are also consistent with image force effects. It is generally accepted that an image force model can be applied to charge injection from electrodes into organic solids.[96] Here, injected charges induce counter charges on the electrode surface, which in turn exert a force on charges being injected away from the electrodes. This so-called image force effect has both negative and positive characteristics with respect to charge injection. At close proximities to the electrode (≤ 1 nm), the charge backscattering region, charges experience strong Columbic forces attracting them back to the electrode, thereby retarding injection. However, if the charges escape this region, they experience a lower barrier and injection is facilitated. The thickness of the present *n*-butyl- and *n*-octylsiloxane SAMs are in the dimensional length scale of typical charge backscattering regions (~ 1 nm).[96] We suggest that holes can therefore be injected with a low barrier substantially through or beyond the backscattering region of the image force field. In this way, hole injection is enhanced as compared to that of bare ITO. Thus, the *n*-butylsiloxane and *n*-octyl SAMs reduce the negative effect of the image force in terms of hole injection. In the case of the thinner (~ 2.8 Å) methylsiloxane SAM deposited on the ITO surface, the negative side of the image force effect should dominate and should retard hole injection. The total current observed in the I−V characteristics of Figure 9 is the sum of the injection current and of the leakage current near either the hole or the electron injection contacts.[97] Based on the above discussion of SAM defects and image force effects, *n*-butyl- and *n*-octylsiloxane SAMs would have larger injection currents and smaller leakage currents versus those of methylsiloxane SAM, and larger total currents, which explains relative the I−V, L−V, and quantum efficiency characteristics in Figure 9.

Comparison of Alkylsiloxane SAMs to TPD-Si$_2$ and NPB-Si$_2$ SAMs as HTLs. Evidence of Significant ITO Anode−HTL Contact Effects on OLED EL Response. The simple treatment of the ITO surface with a saturated hydrocarbon *n*-butyl siloxane monolayer results in a dramatic OLED EL response enhancement (ITO/SAM/Alq vs ITO/Alq OLEDs), and device performance roughly comparable to NPB-only HTL-based OLEDs (ITO/SAM/Alq vs ITO/NPB/Alq OLEDs). These results demonstrate that conventional hole transport layers may be deleted from small molecule OLED structures without major degradative effects on quantum efficiency and luminance, conveying fundamental implications for OLED and HTL design.[98] The favorable performance data for OLEDs fabricated with the alkylsiloxane or triarylamine siloxane-modified ITO anodes and efficient electron injection systems indicate that ITO anode−HTL chemical/physical/electrical contact is a significant factor contributing to effective HTL function, considering the
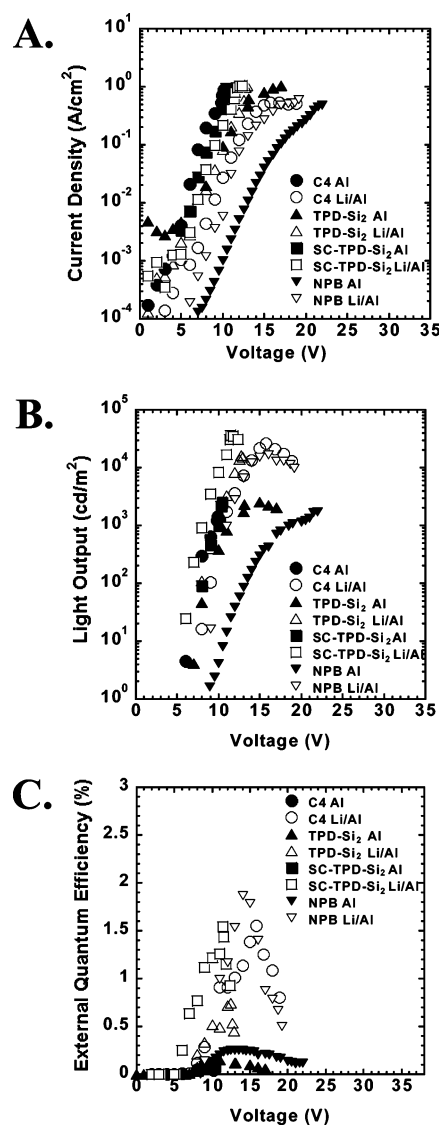
(95) Finklea, H. O. In *Electroanalytical Chemistry*; Bard, A. J., Rubenstein, I., Eds.; Marcel Dekker: New York, 1996; Vol. 19, pp 177−194.
(96) Tutis, E.; Bussac, M. N.; Zuppiroli, L. *Appl. Phys. Lett.* **1999**, *75*, 3880−3882.
(97) Khramtchenkov, D. V.; Bssler, H.; Arkhipov, V. I. *J. Appl. Phys.* **1996**, *79*, 9283−9290.
(98) Chan, I. M.; Hong, F. C. *Thin Solid Films* **2004**, *450*, 304−311

Figure 13. Comparison of responses of OLEDs having the structures ITO/HTL/Alq: 1% DIQA (60 nm)/Al to ITO/(HTL)/Alq: 1% DIQA (60 nm)/BCP:Li (20 nm)/Al, HTL = *n*-butylsiloxane SAM (C4), TPD-Si$_2$ SAM (TPD-Si$_2$), spin-cast TPD-Si$_2$ (SC-TPD-Si$_2$), and NPB alone. (A) Current density versus voltage; (B) luminance versus voltage; (C) external forward quantum efficiency versus voltage.

very different molecular and electronic structures of *n*-butylsiloxane and TPD-Si$_2$, excepting the trichlorosilyl tethers, which covalently graft them to the ITO anode. By carefully controlling the chemisorption process, a simple alkylsiloxane monolayer of appropriate thickness and defect density can replace a conventional HTL constituent with a much more complex structure. This provides motivation to shift research focus from developing hole-transporting materials with new hole transport motifs, to modifying currently available molecules to form stable, robust contacts with ITO anodes.

Alkylsiloxane SAMs as ITO Anode−NPB Interlayers in OLEDs. As noted above, introducing alkylsiloxane SAMs with short alkyl chain lengths as ITO anode−NPB interlayers results in dramatic device performance enhancements versus applying them as the only HTL (Figure 10), which can be explained by a function similar to that of TPD-Si$_2$ and NPB-Si$_2$ as anode−NPB interlayers because (1) direct ITO surface−EML contact in ITO/SAM/Alq OLEDs via SAM defects is avoided by the
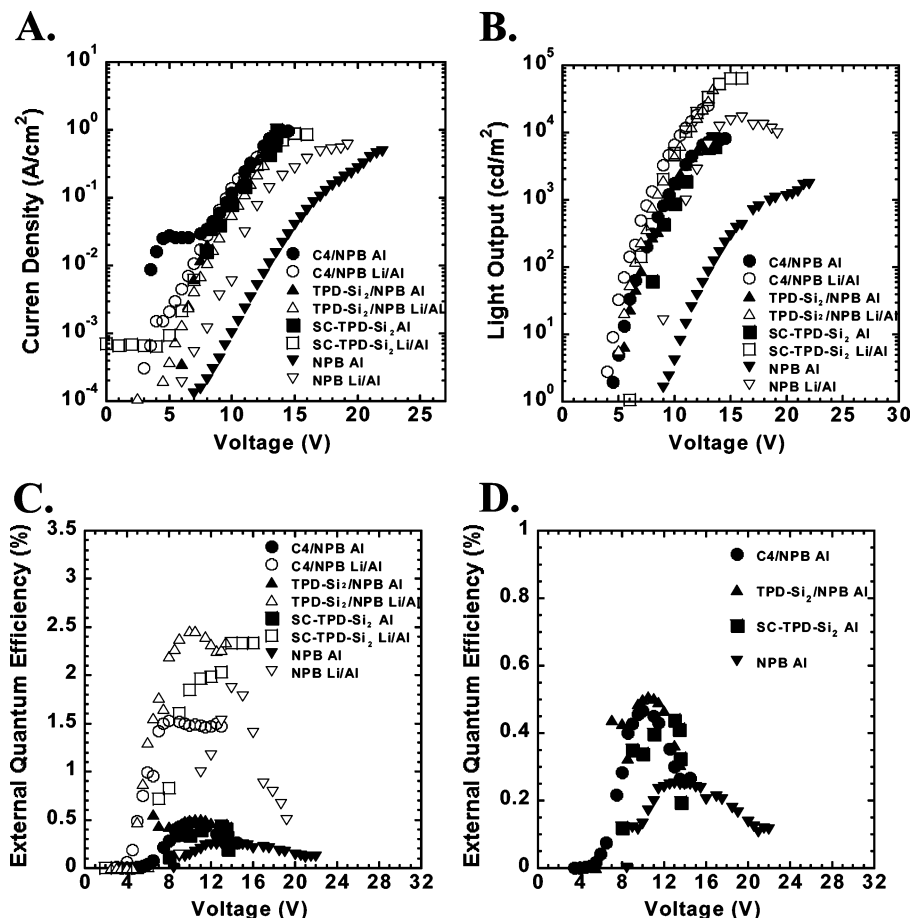
Figure 14. Comparison of responses of OLEDs having structures ITO/(siloxane)/NPB (20 nm)/Alq: 1% DIQA (60 nm)/Al to ITO/(siloxane)/NPB (20 nm)/Alq: 1% DIQA (60 nm)//BCP:Li (20 nm)/Al, siloxane = n-butylsiloxane SAM (C4), TPD-Si$_2$ SAM (TPD-Si$_2$), spin-cast TPD-Si$_2$ (SC-TPD-Si$_2$). (A) Current density versus voltage; (B) luminance versus voltage; (C) external forward quantum efficiency versus voltage; (D) external forward quantum efficiency versus voltage for OLEDs having structures ITO/(siloxane)/NPB/Alq: 1% DIQA/Al.

20 nm thick NPB layer, and electrons should be largely confined to the NPB/Alq interface, increasing the probability of hole-electron recombination, hence EL response; and (2) exciton quenching and/or Alq degradation associated with any remaining silanol functionalities is also avoided by depositing NPB on top of the SAMs. The present device performance improvement versus ITO/NPB devices is therefore primarily attributable to improved ITO anode−NPB contact via surface energy matching.[15] In contrast, employing the thicker n-octadecylsiloxane SAM as an ITO anode−NPB interlayer blocks hole injection, thereby reducing hole-electron recombination efficiency and diminishing device performance.

Balancing Electron and Hole Injection in OLEDs Having Siloxanes as HTLs or ITO Anode−NPB Interlayers. In the OLEDs fabricated with self-assembled or spin-coated triaryl-aminosiloxanes or alkylsiloxanes as HTLs, the effects of electron injection/transport and hole-electron recombination on device performance are very significant (Figure 13). Replacing Alq/Li-doped BCP/Al with simple Alq/Al results in a larger electron injection barrier and lower electron density in the charge carrier recombination region, which diminishes device efficiency and light output. A similar trend is observed when siloxanes are applied as ITO anode−NPB interlayers (Figure 14). Also, note that inserting siloxane interlayers enhances external forward quantum efficiency in the electron-limited Alq/Al OLEDs (Figures 14d and 15), requiring further examination of the
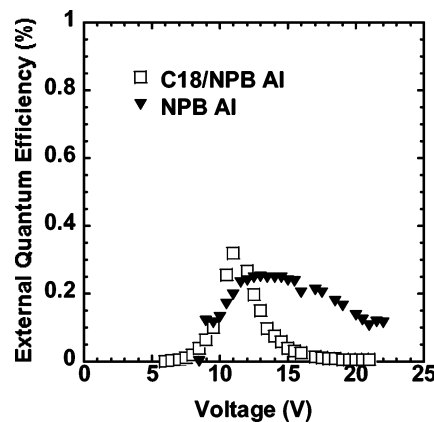

Figure 15. External forward quantum efficiency versus voltage for OLEDs having structures ITO/n-octadecylsiloxane SAM/NPB/Alq: 1% DIQA/Al.

relationship between hole injection and quantum efficiency, particularly in an electron injection-limited scenario.[28,31,70,85,99] Suppression of hole injection is known to ameliorate the imbalance of major (hole) and minor (electron) charge carrier densities near the HTL/EML interface, improving quantum efficiency.[27,31] However, a number of research groups have experimentally observed and theoretically predicted regimes

(99) Zhou, X.; Pfeiffer, M.; Blochwitz, J.; Werner, A.; Nollau, A.; Fritz, T.; Leo, K. *Appl. Phys. Lett.* **2001**, *78*, 410−412.

having increased quantum efficiencies with enhanced hole injection in electron-limited devices.[70,100−103] The former regime is observed when *n*-octadecylsiloxane SAM is inserted as ITO anode−NPB interlayer, and the latter is observed when TPD-Si$_2$ and *n*-butylsiloxane are used as the interlayers, arguing that holes are injected and accumulated at the HTL/EML interface (aided by the hole/exciton-blocking characteristics of BCP), thus altering the internal electrical field, enhancing the electric field drop across the ETL, and thereby enhancing electron injection.[100]

5. Conclusions

ITO anode−HTL contact plays a significant role in OLED EL response. A new strategy in HTL materials development is presented here, focusing on chemical/physical/electrical contact rather than on HTL molecular architecture. In this contribution, traditional HTL molecules such as TPD and NPB are modified with trichlorosilyl groups and can be self-assembled or spin-coated onto the ITO surface, enhancing ITO−HTL contact via

robust covalent bonding. This unique contact effect distinguishes the present HTL materials from traditional ones and results in dramatic OLED device performance enhancement. It is also demonstrated here that alkylsiloxane SAMs can function as HTLs, even though they lack classical hole transport motifs, provided that suitable alkyl chain lengths are chosen. This further evidences the important role of ITO anode−HTL contact in HTL design. The new HTL materials developed here can also be applied as ITO anode−NPB interlayers, further enhancing device performance and representing an effective approach to fabricating OLEDs with high brightness (maximum ∼64 000 cd/m^2), low operating voltage (∼7 V at 300 cd/m^2), and large current efficiencies (∼8 cd/A).

Supporting Information Available: X-ray reflectivity data normalized to the Fresnel reflectivity, for a film formed by self-assembly of TPD-Si$_2$ and NPB-Si$_2$ on Si, respectively. This material is available free of charge via the Internet at http://pubs.acs.org.

JA051077W

(100) Khramtchenkov, D. V.; Bssler, H.; Arkhipov, V. I. *J. Appl. Phys.* **1996**, *79*, 9283−9290.
(101) Burrows, P. E.; Shen, Z.; Bulovic, V.; McCarty, D. M.; Forrest, S. R.; Cronin, J. A.; Thompson, M. E. *J. Appl. Phys.* **1996**, *79*, 7991−8006.
(102) Yang, S.; Wang, Z.; Xu, Z.; Hou, Y.; Xu, X. *Chem. Phys.* **2001**, *274*, 267−273.
(103) Giebeler, C.; Antoniadis, H.; Bradley, D. D. C.; Shirota, Y. *Appl. Phys. Lett.* **1998**, *72*, 2448.